Two-channel Kondo Physics: from Engineered Structures to Quantum Materials Realizations

Stefan Kirchner

Email: `stefan.kirchner@correlated-matter.com`
Zhejiang Institute of Modern Physics, Zhejiang University, Hangzhou, Zhejiang 310058, China
Zhejiang Province Key Laboratory of Quantum Technology and Devices, Zhejiang University, Hangzhou 310027, China

Abstract. The Kondo effect assumes a central role in condensed matter physics. It describes the exchange scattering of electrons with a localized moment and occurs in a wide range of settings from rare earth-based intermetallics to nanotubes and semiconductor heterostructures. A conceptually simple extension of the model, known as the two-channel Kondo model, can give rise to singular scattering and the formation of an unconventional metal. Although the observation of the standard Kondo effect has become ubiquitous, its two-channel counterpart has been proven difficult to realize. This article reviews attempts, challenges, and successes in realizing the two-channel Kondo effect in artificial structures and real quantum materials.

1. Introduction

An important motor of quantum matter research is the need for novel materials for future technological applications. Equally important is the effort to understand the properties of quantum matter in terms of a few comprehensive principles underlying the observed diversity across different material classes. General arguments, *e.g.*, indicate that $4f$ electrons are more localized than $3d$, $5f$, or $4d$ electrons. The interplay between continuous itinerant and local degrees of freedom is a recurrent theme in condensed matter research [1]. This interrelationship has commonly been associated with heavy-electron materials involving lanthanide or actinide ions like Cerium, Ytterbium, or Uranium [2, 3, 4]. There is, however, mounting evidence that also other materials' classes like the cuprates, or iron pnictides are located at the border between electron localization and itinerancy [5, 6, 7]. This proximity to localization appears to be intimately related to the *strange* metal behavior which has been observed in many unconventional superconductors above their superconducting transition temperature T_c [8, 9, 10]. In conventional metals the resistivity (ρ) at sufficiently low temperature (T) displays a quadratic-in-T dependence. This universal low T behavior is a feature of the Landau-Fermi (or simply Fermi) liquid fixed point. In contrast to conventional metals, the T-dependence of the strange metal phase is characterized by a linear-in-T behavior over a wide T region [11]. This behavior is so prevalent that metals which do not display the Fermi liquid phenomenology are commonly known as non-Fermi liquids. The common feature of all metallic non-Fermi liquids is the existence of gapless excitations which do not resemble electrons or holes. This is contrary to the Fermi liquid, where quasi-particles, *i.e.*, quasi-electrons or -holes remain well defined. The Fermi liquid is adiabatically connected to the free electron gas. The strange metal phase appears to be a particular kind of non-Fermi liquid behavior. The similarities between the strange metal phase in the cuprate, pnictide, selenide, and some of the rare earth-based heavy-electron superconductors, as well as the overall comparability of the phase diagrams, *e.g.*, the proximity to magnetism and significance of charge localization, is striking and seems to suggest a common origin across different materials' classes [12, 13]. This observation has motivated a search for routes to non-Fermi liquid behavior.

In the context of lanthanide-based heavy-electron compounds, it is well established that their low T properties are a result of Kondo physics and its interplay with the Ruderman-Kittel-Kasuya-Yosida or RKKY exchange interaction [14, 15, 16]. The competition between the two can also lead to unconventional quantum criticality which, in this context, arises from a critical Kondo destruction and often occurs at the border of magnetism in these heavy-electron systems [17].

The distinguishing feature of Kondo physics is the scattering of electrons and holes at a localized, spin-1/2 moment [2]. This leads to the formation of a Fermi liquid state as $T \longrightarrow 0$ with very strong potential scattering [18]. In a more realistic setting, the degeneracy of the local f ($l = 3$) or d ($l = 2$) eigenstates, reduced by spin-orbit coupling and crystalline electric field effects, should be taken into account. Moreover, more than

one conduction band possibly could couple to the local moment. As a result, a higher-spin multi-channel Kondo model may arise as the proper low-energy model [19].

Under very special circumstances, overscreening of the local moment, see Sec. 2.2, might occur in which case non-Fermi liquid behavior will emerge at sufficiently low T [19, 20]. For a quantum spin of size $1/2$, this situation can occur in the two-channel Kondo (2CK) model and constitutes the conceptionally perhaps simplest route to a singular metallic state with non-Fermi liquid behavior.

A periodic lattice of 2CK scattering centers, *i.e.*, a 2CK lattice, is expected to display features reminiscent of the strange metal phase [21]. This reasoning is further corroborated by the strange metal behavior arising near quantum criticality in the $4f$ electron-based intermetallics, which is driven by a competition of Kondo and RKKY physics. The simplest model that captures such a competition is the two-impurity Kondo model [22]. Its quantum critical point turns out to be equivalent to the 2CK fixed point. This indicates that realizations of the 2CK effect may shed light on how Fermi liquid states give way to strange metal behavior and ultimately promote novel phases, like *e.g.* unconventional superconductivity. Despite its conceptual simplicity, however, the 2CK effect is rather fragile against perturbations and has proven quite difficult to realize.

In this article, I review the 2CK problem and its possible realizations ranging from artificial quantum devices to condensed matter systems. The article concludes with a brief overview of the most recent developments.

2. Kondo Physics

2.1. The single-channel Kondo effect

The scattering of electrons at a magnetic moment $\mathbf{S}$ localized at position $\mathbf{r} = 0$, formed *e.g.* by a transition metal or lanthanide ion immersed in a metal, can be described by

$$H_K^{\text{aniso}} = \sum_{n,k,\sigma} \varepsilon_k^n c_{n,k,\sigma}^\dagger c_{n,k,\sigma} + J_K^\parallel S^z \sum_n s_n^z(\mathbf{r} = 0)$$

$$+ \frac{J_K^\perp}{2} \sum_n \left(S^+ s_n^-(\mathbf{r} = 0) + S^- s_n^+(\mathbf{r} = 0) \right). \tag{1}$$

Here, $\mathbf{S}$ is exchange coupled to the local ($\mathbf{r} = 0$) spin density, $\mathbf{s}(\mathbf{r} = 0) = (s^x, s^y, s^z)(\mathbf{r} = 0)$, of n conduction bands of dispersion ε_k^i ($i = 1, \ldots, n$) via longitudinal and transversal Kondo exchange couplings $J_K^\parallel$ and $J_K^\perp$ respectively. In the case $J_K^\parallel = J_K^\perp$ and for a single conduction band ($n = 1$), the model simplifies to the spin-isotropic Kondo model

$$H_K = \sum_{n,k,\sigma} \varepsilon_k^n c_{n,k,\sigma}^\dagger c_{n,k,\sigma} + J_K \sum_n \sum_{k,k',\sigma,\sigma'} \mathbf{S} \cdot \boldsymbol{\sigma}_{\sigma,\sigma'}^n c_{n,k,\sigma}^\dagger c_{n,k',\sigma'}. \tag{2}$$

For $J_K > 0$, the exchange interaction favors antiferromagnetic alignment while $J_K < 0$ is a ferromagnetic coupling. In Eq. (2), $\boldsymbol{\sigma}$ is a vector formed by the Pauli matrices and $c_{n,k,\sigma}^\dagger (c_{n,k,\sigma})$ creates (destroys) a conduction electron state in band n with lattice momentum k and spin projection σ. The resistivity $\rho(T)$ that follows from the Kondo Hamiltonian displays a peculiar T dependence which is a reflection of the T dependence
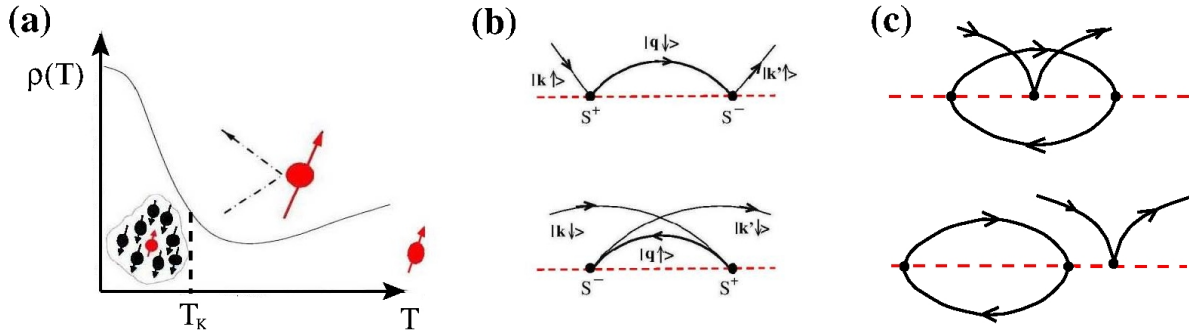
(a)

(b)

(c)

Figure 1. (a) The resistivity $\rho(T)$ of a magnetic impurity imbedded in a metal displays a characteristic temperature (T) dependence due to dynamic spin-flip scattering. At high T, the spin is essentially free. Well below a dynamically generated low-energy scale, T_K, the system of impurity and electrons forms a many-body singlet. As a result, $\rho(T)$ features an enhanced residual $(T = 0)$ resistivity plus $(T/T_K)^2$ corrections. Around the crossover scale T_K, strong spin-flip scattering leads to an increasing ρ with decreasing T. (b) Perturbative contributions to the scattering T-matrix in 2nd order of the exchange coupling J_K. The two diagrams shown yield a logarithmic contribution in energy and form the one-loop contributions which contribute to the scaling equation up to order J_K^2. (c) The two diagrams are of order J_K^3 and form the two-loop contributions for the 2CK effect.

of the scattering T-matrix $(\mathcal{T})$ of the conduction electrons. The T-matrix relates the free conduction electron Green function (g), which describes the propagation of electrons in the absence of the local moment, to the full one (G) via $G = g + g\mathcal{T}g$. The scattering rate, which determines $\rho(T)$, in turn is directly related to the absolute values of matrix elements of $\mathcal{T}$ (in a basis of initial and final states).

Starting from high T, the scattering rate decreases with decreasing T as is common for metals, before increasing again near some characteristic energy, called the Kondo temperature (T_K), see Figure 1(a). This energy scale is dynamically generated and characterizes the crossover from the local moment regime at high T, where the spin susceptibility is Curie-like to a strongly correlated regime, where the local moment is confined to a many-body singlet formed with the conduction electrons. This regime is characterized by a Pauli-like spin susceptibility with an enhanced density of states at the Fermi energy that scales with $1/T_K$. This behavior is reminiscent of a Fermi liquid, the generic ground state behavior of most ordinary metals and which is characterized by the existence of well-defined quasiparticles [23]. It is a distinctive feature of the Kondo effect that an adequate description of the crossover from the local moment behavior to the low T regime is non-trivial. Indeed, it has long been recognized that the application of perturbation theory to the Kondo Hamiltonian leads to divergent results [24]. This can be seen by analyzing the two Feynman diagrams shown in Figure 1(b) which represent contributions to $\mathcal{T}$ in 2nd order perturbation theory in terms of the exchange coupling J_K. The black continuous line in these diagrams represents conduction electron states while the dashed line symbolizes the possible states of the local moment. A dot symbolizes the interaction; a diagram with two dots is thus proportional to J_K^2.

An important feature of the Kondo effect is its quantum mechanical nature that is reflected in the behavior of the two processes shown in Figure 1(b). It involves electrons (upper diagram) and holes (lower diagram). The sum of the two diverges logarithmically as the energy of the scattering electron approaches the Fermi energy [2]. This divergence is a consequence of the existence of a local quantum algebra, encoded in the commutators for the SU(2) generators S^+, S^-, and S^z of the local moment **S** and its coupling to a continuous bath of fermion states. Similar divergencies occur in all higher orders of perturbation theory and signal the instability of the starting point, *i.e.*, the weak coupling fixed point with $J_K \approx 0$. As a result, the system dynamically generates a low-energy scale, the Kondo temperature

$$T_K = D\, e^{-1/N_0 J_K}, \tag{3}$$

where D is the half-bandwidth of the conduction electron band and N_0 is its density of states at the Fermi energy.

This result motivated the perturbative renormalization group (RG) treatment of the Kondo problem and lead to the poor man's scaling equation for the effective exchange coupling [25, 26]

$$\frac{dJ}{dD} = -N_0 \frac{J^2}{D}, \tag{4}$$

which relates changes $D \to D + dD$ in the cutoff to those in the exchange coupling J while leaving $\mathcal{T}(\epsilon)$ for energies below the reduced cutoff invariant. Equation (4) is based on the diagrams shown in Figure 1(b). This creates a manifold of Kondo systems with identical low-energy behavior, parameterized by

$$J(D) = \frac{J_K}{1 - N_0 J_K \ln\left(\frac{D(J_K)}{D}\right)}, \tag{5}$$

where J_K is the original exchange coupling and $D(J_K)$ the associated band cutoff.

The right-hand side of Equation (4) only includes terms up to second order in J which is a reflection of its perturbative origin. Note, that the linear-in-J term vanishes. This implies that the Kondo exchange coupling is marginally irrelevant for $J < 0$ and marginally relevant for $J > 0$. It follows from Equation (5) that for ferromagnetic couplings ($J_K < 0$) $J \to 0$ as $D \to 0$ while J becomes singular as D approaches T_K for $J_K > 0$, *i.e.* antiferromagnetic couplings. This divergence for $J_K > 0$ is artifical and signals that an inclusion of higher-order terms beyond the diagrams shown in Figure 1(b) is necessary [27].

A proper incorporation of higher order terms was ultimately accomplished by the development of K. Wilson's RG which showed that $J(D) \to \infty$ as $D \to 0$ is indeed the correct behavior: The ground state of the $J_K > 0$ Kondo problem is that of a many-body singlet. Moreover, the excitations on top of the ground state are of fermionic nature [28]. In the low-energy limit, the Kondo impurity only acts as a very strong potential scatterer close to its unitary limit, where the conduction electrons experience a scattering phase shift of $\pi/2$ in the Kondo limit [18].

The poor man's scaling approach also established an equivalence between the $J_K > 0$ Kondo model and the one-dimensional Ising model with periodic boundary conditions and a ferromagnetic long-ranged interaction that falls off quadratically with distance along the ring [25, 26]. Integrating over domains in the partition function of this long-ranged Ising model leads to an equivalent representation in terms of kinks and anti-kinks associated with the domain walls in terms of the Ising spin representation. Thus, the Kondo model is also equivalent to a one-dimensional Coulomb gas with a logarithmic interaction among the $+$ (kink) and $-$ (anti-kink) charges [29].

One of the attractive features of the Kondo effect is that it constitutes a phenomenon of strong electron correlations that is located right at the verge of solvability. The problem can be tackled by a number of methods, including essentially exact approaches, like conformal field theory and Bethe ansatz solutions [30, 31, 32, 33, 34], that pertain in certain limits. For a special and non-universal value of the longitudinal exchange coupling $J_K^{\parallel}$, the anisotropic Kondo model can be mapped to a resonant level model, *i.e.*, a non-interacting model with resonant tunneling at the Fermi energy [35]. This particular limit of the anisotropic Kondo model is known as the Toulouse point, at which the model can be solved straightforwardly.

The generalization of Equation (4) to the anisotropic Kondo model, where $J_K^{\perp} \neq J_K^{\parallel}$, yields $dJ^{\parallel} = -N_0(J^{\perp})^2/D$ and $dJ^{\perp} = -N_0 J^{\parallel} J^{\perp}/D$. These two equations imply that $(J^{\parallel}/J^{\perp})2 \to 1$ as the strong-coupling fixed point is approached, *i.e.*, the low T fixed point displays symmetry restoration [36].

The Kondo effect is an example of the richness that arises from the coupling of a discrete degree of freedom to a gapless bath of quantum fields. For it to form, a local quantum algebra, *e.g.* a local SU(2) associated with the localized moment, is required, which, in combination with the Fermi edge of the conduction electron bath, leads to the characteristic logarithmic divergencies in the perturbative treatment underlying Equations (3) and (4).

Note, that the inclusion of the cubic term in Equation (4) would automatically imply the existence of a critical, non-zero $J^{\star} < \infty$ at which

$$\left. \frac{dJ}{dD} \right|_{J^{\star}} = 0. \tag{6}$$

This would imply the existence of a further fixed point in addition to the weak-coupling ($J = 0$) and strong-coupling ($J \to \infty$) fixed points. Moreover, non-Fermi liquid-like powerlaw behavior would be expected in the vicinity of $J^{\star}$. Whether such a finite-coupling fixed point is an artefact of the perturbative treatment or if it could arise and if so, under which conditions, has been first analyzed by Noziéres and Blandin [19] and independently by Zawadowski [37].

2.2. The two-channel Kondo effect

The more realistic model of a magnetic moment $\boldsymbol{S}$ of size S, exchange coupled to n conduction bands via anti-ferromagnetic couplings, Equation (1), allows for a much

richer behavior than the Kondo model H_K of Equation (2). Its properties were analyzed in detail in [19]. A stability analysis of the strong-coupling fixed point shows that three qualitatively different cases may occur, depending on the ratio of n and S.

The strong-coupling fixed point for $n = 2S$ is a singlet state that is formed by the local moment and the conduction electrons. This leads to a pure potential scatterer similar to the situation in the standard Kondo model, Equation (2), discussed above. This is the case of perfect screening.

Underscreening occurs if the size of the local moment exceeds $n/2$. In that case, the ground state near the strong-coupling fixed point is characterized by a local moment with a reduced effective spin $S_{\text{eff}} = S - n/2$ provided the initial Kondo exchange coupling J_K is of sufficient strength. As it turns out, the conduction electrons experience a ferromagnetic effective exchange interaction with this S_{eff}. It then follows from Equation (5) that this effective exchange coupling J_{eff} tends to zero at lower and lower energies analogous to the behavior found in the ferromagnetic Kondo model. As a result, the strong-coupling fixed point with an asymptotically decoupled S_{eff} is stable.

In the opposite case, where $n > 2S$, the conduction electrons overcompensate the local moment and generate a local effective moment $S_{\text{eff}} = n/2 - S$. In this case, the effective exchange interaction between S_{eff} and the conduction electron bands turns out to be antiferromagnetic. From Equation (5), we thus conclude that this effective exchange coupling J_{eff} will scale to larger values as D is being reduced. In terms of the original coupling J_K this corresponds to an effective reduction, as $J_{\text{eff}} \sim 1/J_K$. The strong-coupling fixed point in the overscreened case is thus unstable, but so is the weak coupling fixed point [20]. Noziéres and Blandin thus concluded that in this case the system flows to an intermediate coupling fixed point characterized by a critical effective coupling $J^\star$ that can be described by the scaling equation [19]

$$\frac{dJ}{dD} = -N_0 \frac{J^2}{D} + nN_0^2 \frac{J^3}{D},$$ (7)

where the cubic contribution originates from the processes encoded in the diagrams shown in Figure 1(c). The critical value $J^\star = 1/nN_0$, obeying $\frac{dJ}{dD}|_{J^\star} = 0$, marks the intermediate coupling fixed point. The overall correctness of this conclusion and the underlying stability analysis has been confirmed *e.g.* through numerical renormalization group (NRG) calculations [38].

The physical properties of the critical fixed point at $J^\star$ are fundamentally different from those of the Fermi liquid fixed point that resides at strong coupling $J \to \infty$. Its critical features are reflected in the scaling behavior of physical quantities in its vicinity, *i.e.*, at energies and temperatures well below the Kondo temperature T_K. In Table 1, a comparison is made between the physical quantities near the one-channel strong-coupling ($S = 1/2$, $n = 1$) and the 2CK ($S = 1/2$, $n = 2$) fixed points. Most notably in this list might be the residual $T = 0$ impurity entropy $S(T = 0) = \ln \sqrt{2}$ associated with the 2CK fixed point [39, 40, 41, 42]. This impurity entropy is defined as the difference of entropies of the full Hamiltonian and the conduction electron contribution alone. Likewise, the specific heat behavior quoted in Table 1 refers to the impurity specific

heat which is defined in an analogous manner. The $T = 0$ limit of $\rho(T)$ for the 2CK model has been obtained using conformal field theory (CFT) methods [30, 31]. In

Physical quantity	1CK effect	2CK effect
C/T	$\sim 1/T_K$	$\sim \ln(T/T_K)$
$S(T = 0)$	0	$\frac{1}{2}\ln(2)$
$\chi(T \ll T_K)$	$\sim 1/T_K$	$\sim \ln(T/T_K)$
$\rho(T) - \rho(0)$	$\sim \left(\frac{1}{T_K}\right)^2$	$\sim \left(\frac{1}{T_K}\right)^{1/2}$

Table 1. A comparison of the one- vs 2CK effect: low T specific heat contribution divided by T (also known as the γ coefficient), residual entropy, low T spin susceptibility and low T resistivity.

contrast to the single-channel Kondo case which leads to strong elastic scattering in the $T = 0$ limit, multi-channel Kondo impurities generate inelastic scattering even in the $T = 0$ limit [18, 41].

As it turns out, the Toulouse limit of the one-channel Kondo model can be generalized to its two-channel counterpart [43] but extra effort is required to obtain the correct behavior of physical quantities like *e.g.* the spin susceptibility and the specific heat [44]. This particular case of a 2CK model is also known as the Emery-Kivelson point.

The CFT description of the 2CK fixed point also establishes which couplings would drive the system away from the fixed point, *i.e.*, which perturbations are relevant. As the critical point arises out of a competition of two channels which independently attempt to screen the local moment, a perfect frustration between these channels is needed to reach the multi-channel Kondo fixed point. An imbalance in either the dispersion ε_k^n of the different bands or the coupling strength J_K with the local moment will ultimately favor one channel over the other. Thus, a channel anisotropy constitutes a relevant perturbation at the intermediate fixed point. Another vital requirement is that no direct coupling between the different channels can exist except through the local moment itself, if the 2CK fixed point is to be reached [42, 45].

In spite of the fact that the 2CK effect is conceptually possibly the simplest route to a metallic non-Fermi liquid ground state, the requirements necessary to reach this fixed point put severe constraints on possible physical realizations. This is in stark contrast to the one-channel Kondo effect that has been realized in a great variety of systems including semiconductor heterostructures, nanotubes, single molecules, molecules adsorbed on surfaces, magnetic impurities in metals.

3. The Kondo Effect in Quantum Dots and Nanostructures

3.1. Artificial atoms: quantum dots, molecular junctions, nanotubes

The possibility of realizing Kondo scattering in nanostructures or 'artificial atoms', like quantum dots and molecular junctions was first pointed out in Refs. [46, 47]. The observation of Kondo physics in quantum dots was later accomplished by several groups [48, 49, 50]. Subsequently, the engineering of Kondo physics in more invovled nanostructures and single-molecule transistors was achieved [51, 52]. For a review of Kondo physics in quantum dots, see *e.g.* [53].

Two important energy scales of quantum dots that play a central role in realizing Kondo scattering are the energy level spacing Δ and the charging energy E_C. A non-vanishing Δ is a consequence of the electron confinement within the dot. For energies that are small compared to Δ, quantum dots can be modeled in terms of the single-level Anderson model (Figure 2),

$$H_{\text{AM}} = \sum_{\sigma} \left(\varepsilon_d + eV_G\right) d_\sigma^\dagger d_\sigma + U d_\uparrow^\dagger d_\downarrow^\dagger d_\downarrow d_\uparrow$$

$$+ \sum_{\lambda=S,D} \sum_{k,\sigma} \varepsilon_{\lambda,k} c_{\lambda,k,\sigma}^\dagger c_{\lambda,k,\sigma} + \sum_{\lambda,k,\sigma} \left(t_\lambda c_{\lambda,k,\sigma}^\dagger d_\sigma + \text{h.c.}\right), \quad (8)$$

where U is a measure of the Coulomb repulsion between the dot electrons with spin projection $\uparrow$ and $\downarrow$ while ε_d is the energy of the single-particle level closest to the Fermi energy E_F of the source ($\lambda = S$) and drain ($\lambda = D$). The gate voltage V_G allows to tune this energy. The dispersion in lead λ is given by $\varepsilon_{\lambda,k}$ and t_λ is the coupling strength between states in lead λ and the dot. For simplicity, this coupling is taken to be local and spin-independent. The charging energy E_C is defined as the energy difference between the states with $n+1$ and n electrons on the dot: $E_C = E(n+1) - E(n)$. From H_{AM}, one finds

$$E_C = E(n+1) - E(n) = \varepsilon_d - eV_G + nU \quad (9)$$

(for $t_\lambda = 0$). This expression is easily generalized to a quantum dot with several levels.

In the Coulomb blockade regime, charge transfer between the leads and the dot is energetically suppressed. As a result, real charge fluctuations can essentially be neglected and a wide parameter range in ε, U, and $\Gamma_\lambda = \pi|t_\lambda|^2 N_0^\lambda$ exists, where H_{AM} at low energies is well described by the spin-isotropic Kondo model. This remains true even though the average local occupation of the dot may be smaller than 1, indicating mixed valency. In this regime, integrating out virtual charge fluctuations through a Schrieffer-Wolff transformation takes H_{AM}, Equation (8), into the Kondo model [56, 57]. Here, N_0^λ is the density of states (DOS) of lead λ at E_F.

It is interesting to note that the Anderson model of Equation (2) can also develop a Kondo effect in its charge sector. At half-filling, where $\varepsilon_d + U/2 = -eV_G$, an SU(2) symmetry in the charge sector ensure the degeneracy of the empty and doubly occupied local states. For negative values of the Coulomb matrix element U, these two states form the local ground state. Again, a Schrieffer-Wolff transformation can be employed
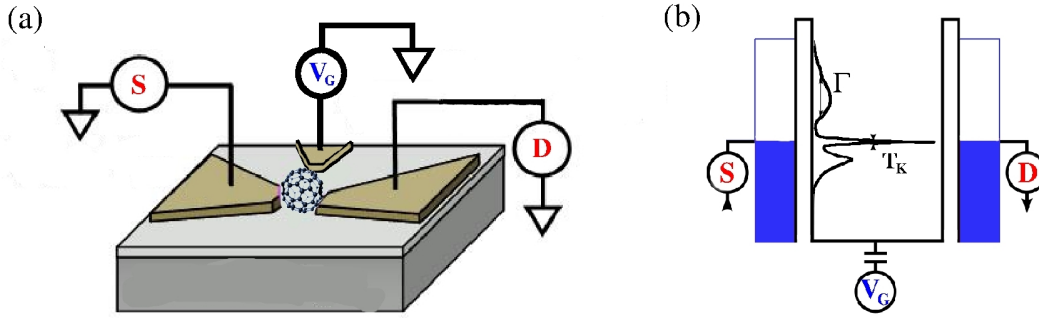
(a)

(b)

Figure 2. (a) Sketch of a quantum dot formed by a C_{60} molecule and attached to two leads, labeled S and D. An additional gate electrode allows to tune the system through one or several Coulomb blockade valleys as a function of the gate voltage V_G. (Adapted from [54]) (b) At energies and temperatures small compared to the level spacing the effective model for a quantum dot is the Anderson impurity model. The gate voltage V_G shifts the energy of the energy level of the dot with respect to the Fermi energy E_F of the leads and possibly the matrix element between lead states and the dot level. The sharp resonance right at E_F is the Kondo resonance and at $T << T_K$ possesses a full width at half maximum of the order of T_K. (Sketch adapted from [55])

to integrating out virtual spin fluctuations and a Kondo model emerges in the low-energy charge sector. The associated Kondo effect is known as the 'charge Kondo effect' [58].

In contrast to the case of a magnetic impurity immersed in a metallic host, for the Kondo effect in quantum dots, it is not $\rho(T)$ that shows a characteristic increase as T is lowered through T_K, as shown in Figure 1(a), but the conductance $G(T)$ that passes through the system. $G(T)$ increases up to its maximal value of $G(T = 0) = 2G_0$, where $G_0 = e^2/h$ is the quantum of conductance and the factor of two accounts for the spin degree of freedom. The maximal G is reached at $T = 0$ for the particle-hole symmetric H_{AM}, where $2\varepsilon_d + U = 0$ and for symmetric coupling $\Gamma_D = \Gamma_S$. Away from particle-hole symmetry, the Schrieffer-Wolff transformation also generates a potential scattering term which reduces the conductance slightly in accordance with Friedel's sum rule [59]. For non-symmetric coupling the conductance is further suppressed by a factor $2\Gamma_D\Gamma_S/(\Gamma_D + \Gamma_S)$.

Figure 2(b) shows the interacting local DOS of the quantum dot with two single-particle peaks, related to the singly and doubly occupied states, and located well below and well above E_F. These two peaks possess a characteristic width $\Gamma = \Gamma_D + \Gamma_S$. At $T \ll T_K$, the local DOS displays a sharp resonance of characteristic width T_K that is pinned at close vicinity of E_F and acquires a value at E_F and $T = 0$ that is enforced by Friedel's sum rule.

Depending on the particular realization of H_{AM}, the corresponding characteristic energy scales of E_C, U, t_S, t_D and $1/N_0$ can vary considerably. Together, these parameters determine the Kondo energy scale T_K. For semiconductor heterostructures [48, 49, 50] the resulting T_Ks are comparatively small, *i.e.*, typically of the order of 1K and below. These structures can, on the other hand, be very well characterized in
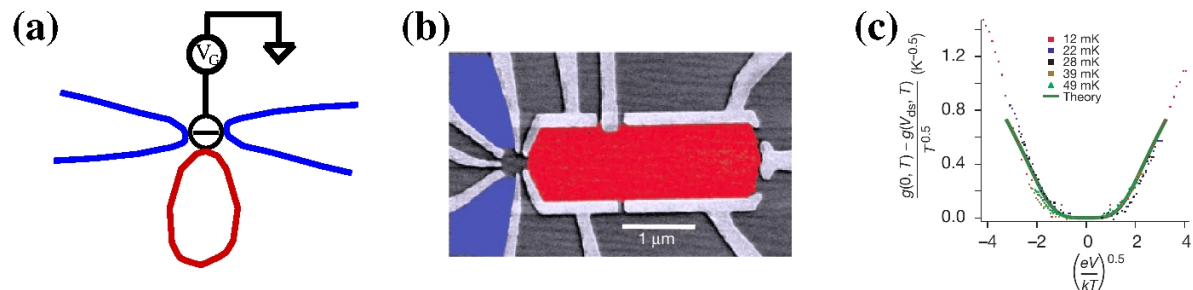
(a)

(b)

(c)

Figure 3. Realization of the magnetic 2CK effect in a semiconductor heterostructure. (a) Sketch of the setup with a large but finite quantum dot (in red), the source and drain lead (in blue). The small quantum dot in the middle confines the local, Kondo-active degree of freedom. (b) Actual realization of the system by the Stanford group. The color coding corresponds to that in (a). (c) The conductance well below T_K displays the characteristic $\sqrt{T}$ behavior on top of a residual conductance and possesses V/T-scaling, where V is the bias voltage between source and drain. (Data in (b) and (c) taken from [66])

terms of the parameters of the effective Anderson Hamiltonian H_{AM}. This facilitates a comparison with theoretical models. The Kondo effect has also been realized in carbon nanotubes where the corresponding energy scales result in T_Ks of the order of 10K [60]. The highest Kondo temperatures have been realized in single molecule devices where T_Ks around 100K and higher are possible [61]. Obtaining a full characterization of these molecular systems remains, however, a challenge [54, 62]. Moreover, due to the larger energy scales in atomic and molecular systems, one is typically confined to stay within one Coulomb valley.

The Kondo effect has even been realized in artificial atoms attached to ferromagnetic leads [63, 64] which allows for new types of quantum critical phenomena like, *e.g.*, the quantum critical destruction of Kondo screening due to the coupling to ferromagnetic spin waves in the leads [65, 57].

One may wonder why the setup shown in Figure 2 with source (S) and drain (D) leads as two screening channels does not lead to a 2CK model but instead constitutes a realization of the one-channel case. As it turns out, when performing a Schrieffer-Wolff transformation, the *mixing terms* $t_D t_S^*$ and $t_S t_D^*$ ensure that only the symmetric combination of S and D couples to the dot, while, for identical leads, the anti-symmetric combination completely decouples from it. This leads to a standard (one-channel) Kondo model.

3.2. Multi-channel Kondo physics in engineered structures

3.2.1. Two-channel Kondo effect in a small quantum dot The applicability of the single-channel Anderson model as the proper low-energy model of small quantum dots as depicted in Figure 2 is restricted to energies that are small compared to the energy level spacing of the dot. Moreover, a vanishing bias voltage $V = E_F^S - E_F^D$ between S and D leads is required, as for $V \neq 0$, the decoupling of the anti-symmetric combination

no longer fully applies. The non-vanishing of $t_S t_D^*$ and $t_D t_S^*$ ensures that the Anderson model with source and drain leads can be mapped to the one-channel Kondo model. Obviously, a vanishing of these terms implies $G(T, V) \equiv 0$. In order to generate the 2CK effect in these quantum dots, a situation is required where the mixing terms vanish.

In 2003, Y. Oreg and D. Goldhaber-Gordon proposed a realization of a magnetic 2CK model [67]. Their proposal is based on an ingenious idea of how to suppress the mixing terms and is sketched in Figure 3(a): The quantum dot is coupled to S and D leads, as before, but also to an additional large but finite dot, which is characterized by a non-vanishing charging energy E_C^L and energy level spacing Δ^L. The E_C^L of this large dot will tend to suppress electron transfer from the leads to the large dot once $k_B T \ll E_C^L$ (k_B is the Boltzmann constant) is satisfied and therefore the mixing terms will be suppressed for sufficiently low T. As a result, this setup is expected to display 2CK physics at energies and temperatures well below E_C^L. On the other hand, at energies and for $k_B T$ large compared to E_C^L, the large dot will simply act as yet another lead and renormalize the effective exchange coupling constant correspondingly. The resulting flow towards the strong-coupling fixed point can be followed up to energies of the order of E_C^L. As Oreg and Goldhaber-Gordon showed [67], the system at this energy scale is effectively described by

$$H_{\text{2CK}} = \sum_{k,\sigma} \sum_{\lambda=S,D,a} \varepsilon_{k,\lambda} f_{k,\sigma,\lambda}^\dagger f_{k,\sigma,\lambda} + u_a (n_a - \mathcal{N}_a)^2 + \sum_{\Sigma} \varepsilon_d d_\sigma^\dagger d_\sigma$$
$$+ J_a \boldsymbol{S} \cdot s_a(0) + J_c \boldsymbol{S} \cdot s_c(0), \tag{10}$$

which is equivalent to the 2CK Hamiltonian where the label $\lambda = S, D, a$ refers to source ($\lambda = S$), drain ($\lambda = D$), and large quantum dot ($\lambda = a$) parts. In Equation (10), $s_c(0)$ denotes the spin density of the symmetric combination of S and D states at the site of the small dot, where the Kondo-active degree of freedom is located. To ensure that the 2CK effect can be reached, $J_a = J_c$ has to be ensured via a judicious tuning of additional gate electrodes. For all this to apply, the level spacing Δ^L has to be sufficiently small. This leaves a finite energy range $\Delta^L < \varepsilon < E_C^L$ in which the flow towards the 2CK fixed point should be observable [67]. Unfortunately, Δ^L and E_C^L are not independent; a tiny Δ^L implies a small E_C^L.

The proposal by Oreg and Goldhaber-Gordon was subsequently realized by the Stanford group and 2CK behavior of the conductance $G(T, V)$ was indeed observed [66, 68]. Figure 3(b) shows the semiconductor heterostructure with the large and small dots and source and drain lead. The color coding of the sketch in Figure 3(a) is such that it reflects that of Figure 3(b). The conductance $G(T, V)$ near the 2CK fixed point is predicted to behave in a singular fashion, *i.e.*, as

$$G(T, V = 0) = G(T = 0, V = 0) - \tilde{a}\sqrt{T/T_K}, \tag{11}$$

with $G(T = 0, V = 0)$ as the residual, $T = 0$ conductance at vanishing bias voltage V and where $\tilde{a}$ is a numerical prefactor. This behavior is the analog of the T dependence of $\rho(T)$ listed in Table 1. The T dependence is in both cases inherited from that of the conduction electron T-matrix $\mathcal{T}$. A powerlaw behavior similar to

that of the T dependence is also expected for the V dependence of the conductance: $G(T = 0, V) - G(T = 0, V = 0) \sim \sqrt{V/T_K}$. As shown in Ref. [66] and reproduced in Figure 3(c), such a scaling behavior is indeed observed. The ensuing V/T scaling of $G(T, V)$ is further evidence for 2CK scaling in the experiment of Ref. [66].

3.2.2. Two-channel Kondo effect in a large quantum dot   In the 2CK realization of Ref. [67, 66], a large quantum dot serves as a screening channel in the dynamic energy range between Δ^L and R_C^L. Interestingly, such a large dot with a non-vanishing E_C and a tiny Δ, as shown in Figure 4, can itself also become a source of Kondo scattering, when coupled to a reservoir of gapless electronic states [69, 70, 71].

In this realization of the Kondo model, the charging state of the large dot plays the role of the (pseudo-)spin degree of freedom. In terms of this pseudospin variable, the tunneling of electrons in and out of the dot become Kondo exchange processes. The whole setup, shown in Figure 4(a), is therefore equivalent to a spin-anisotropic Kondo model. The anisotropy is a consequence of the origin of the pseudospin. The charge degree of freedom in this model lacks the full SU(2) symmetry.

As the gate voltage V_G is tuned, the system transitions through different Coulomb blockade valleys and regions where the average charge $\langle N \rangle$ on the dot will change from n to $n+1$. In the middle of such a region, at $V_G^\star$ one has $\langle N(V_G^\star) \rangle = n+1/2$. Changing V_G away from $V_G^\star$ breaks the degeneracy between the two charging states. The gate voltage $\delta V_G = V_G - V_G^\star$ acts as an effective magnetic field within this pseudospin representation. The Kondo effect in this system leads to subtle logarithmic behavior in

$$\frac{\partial \langle N \rangle}{\partial \delta V_G} \sim \ln \left(\delta V_G \right). \tag{12}$$

With the help of electrodes, the properties of the tunnel contact can be modified in order to tune the number of modes or channels coupled to the dot. The modes are labeled by the quantized transverse momentum that results from the confinement generated by the tunnel contact.

In order to realize the 2CK effect, a second degenerate screening channel is required. The perhaps most natural way to achieve this is via the spin degree of freedom of the electrons. The degeneracy of the spin channels is easily ensured by time-reversal invariance in the absence of magnetic fields. Alternatively, different charge channels could be coupled to the quantum dot. This may have the practical advantage that additional electrodes could be used to tune the system to the required equal tunneling coupling for both channels. A second lead is also required in order to probe for the presence of 2CK correlations via conductance measurements.

At the charge degeneracy point, $\delta V_G = 0$, $G(T)$ should vanishes in the scaling regime as $G(T) \sim T$ [71, 73].

A particular feature of this anisotropic Kondo model is that it is placed right at the 2CK analog of the Toulouse point, which is also known as the Emery-Kivelson point, which was briefly discussed above [43].
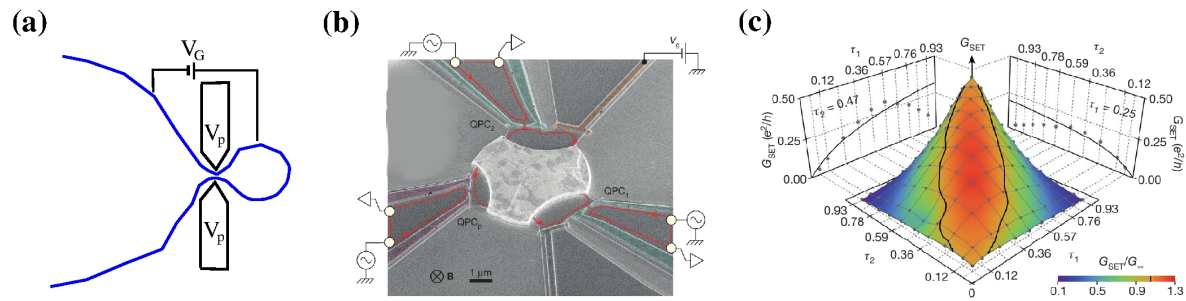
(a)   **(b)**   **(c)**

Figure 4. Kondo scattering between charging states of a large quantum dot: (a) Sketch of the setup: a large quantum dot is coupled to a lead. A gate electrode allows to tune the average number of electrons on the dot via V_G. (b) Realization of Matveev's proposal using semiconductor/metal hybridstructures: a metallic dot connected to quantum point contacts which in turn are attached to leads formed by two-dimensional electron gas (2DEG) states as in Figure 3. (c) Contour plot of the conductance $G(\tau_1, \tau_2)$ as function of tunneling barrier strengths τ_i ($i = 1, 2$) at $T = 11.5$mK. For $\tau_1 \neq \tau_2$, one of the two channels will dominate while the other decouples as $T \to 0$. At the 2CK (Data in (b) and (c) taken from [72]).

The underlying assumptions in Matveev's mapping onto the Kondo model are that the Δ of the dot is negligible and that $k_B T < E_C$. As mentioned earlier, these two conditions are not independent and a vanishing Δ would also imply a diminished E_C. Moreover, the number of modes in the lead (or leads) coupling to the large dot should be small and any channel anisotropy between these couplings need to be avoided if the 2CK fixed point is to be reached. This demand of high control and characterization suggests the use of semiconductor heterostructures for possible realizations of Matveev's proposal but the resulting Δs are generally too large. Metal-based dots on the other hand avoid this problem but make the creation of judiciously tuned contacts very difficult [74]. Additional practical challenges concern the energy dependence of the tunneling barriers, which, if present, may restrict the dynamic range for 2CK scaling as well as the identification of $V_G^\star$ from the conductance alone, based on theoretical expectations.

These concerns not withstanding, Iftikhar et al. managed to realize this charge-version of the 2CK effect [72]. Their approach is based on metal-semiconductor hybrid structures of the type shown in Figure 4(b) to combine the advantages of both structures. The experiment is performed in a large magnetic field to remove the spin degree of freedom [72]. Spatially separated leads act as independent screening channels. This allows for a realization of the multi-channel Kondo model with more than two channels. The situation shown in Figure 4(b), *e.g.*, features three leads [72]. If one of the three contacts is closed, the system can be tuned to the 2CK fixed point at which $G(T) \sim T$ was observed [75].

3.2.3. Carbon nanotubes and graphene The possibility to generate a 2CK effect in carbon nanotubes has been proposed in Ref. [76]. This proposal involves a short nanotube and a filler atom, placed within the nanotube, that possesses a spin-1/2

moment. This composite system is then coupled to two semi-infinite nanotubes, acting as leads, similar to the source and drain gates discussed above. The two degenerate screening channels in this proposal are linked to the degeneracy of two inequivalent valleys at the corners of the hexagonal Brillouin zone of graphene. The existence of the valley degeneracy is a consequence of the sublattice structure of graphene and thus symmetry protected. As a carbon nanotube is a rolled up sheet of graphene, one can obtain the band structure of a nanotube from that of graphene with appropriate boundary condition. This process will preserve the valley degeneracy. In order to ensure that both screening channels will couple equally to the spin-1/2 moment in order to reach the 2CK fixed point, a half-filled, spatially uniform ($l = 0$) wave function is required to carry the moment of the filler atom. So far, no experimental realizations of this proposal has been reported.

An earlier proposal for 2CK physics in graphene was based on a largely similar idea [77]. A magnetic moment-carrying atom would be placed in the center of the unit cell of graphene, so that a 2CK model would arise due to the inequivalent valleys. The linear dispersion near the Dirac points in graphene results in a density of states of conduction electrons which vanishes in a linear fashion. The resulting 2CK model would thus be a pseudogap 2CK model [78]. No realization of this proposal has so far been reported. Such a setup could be probed using scanning tunneling spectroscopy, where a metallic tip is placed above the moment-carrying adatom. The tunneling current would measure the local density of states and possibly contain 2CK signatures. One possible concern with this proposal is that any direct tunneling between tip and the graphene substrate would drive the system away from the 2CK fixed point.

4. Defects in Quantum Materials

Despite considerable efforts and the identification of a number of potential candidates, no fully convincing and universally accepted and undisputed realization of the 2CK effect in real materials has been identified so far. In contrast to real materials, semiconductor/metal-hybrid heterostructures allow for a high degree of device characterization and a deliberate tuning of $\tilde{\varepsilon}_d = \varepsilon_d + eV_G$ and t of the effective Hamiltonian, Eq. (8). In generic materials, these quantities are hard to tune and even extracting their values is difficult.

On the other hand, the realizations of the 2CK effect in the engineered structures discussed in the previous section require a finite charging energy E_C and at the same time a tiny level spacing Δ. This results in only an intermediate dynamic range from Δ to E_C over which 2CK scaling can be observed and small Kondo temperatures T_K of order 1K and below.

Although, the 2CK effect was originally discussed in the context of local moments in metals [19] there does not seem to exist a widely accepted realization of the 2CK impurity model in generic quantum materials. Yet, a direct and convincing demonstration that the 2CK fixed point can exist and is experimentally reachable is highly desirable and
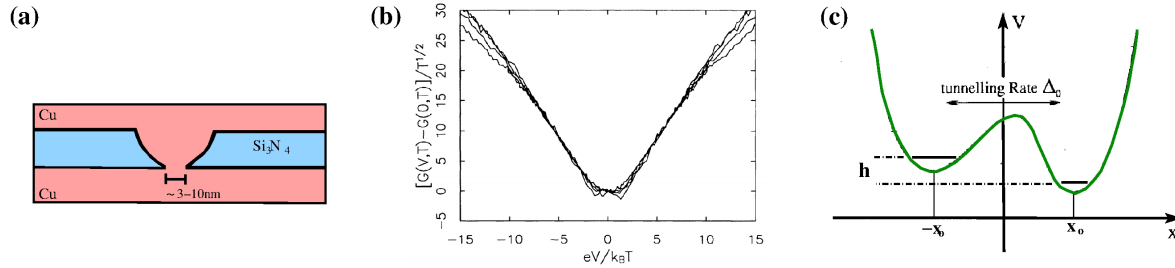
(a) **(b)** **(c)**

Figure 5. Point contact study of Refs. [79, 80]: (a) Sketch of a metallic point contact with a high degree of structural disorder in the metal constriction. (b) The zero-bias anomaly observed by Ralph and Buhrmann scales with exponent $1/2$ in temperature and bias voltage and is compatible with a $T_K \approx 3.5$K. ((a) and (b) taken from [80]) (c) Sketch of a double well potential. This gives rise to a two-level system which serves as a model for the tunneling centers in the nano-constriction.

would constitute a stringent test of our understanding of the interplay of local and itinerant quantum degrees of freedom that is central to strongly correlated electron systems. As a result, a number of candidate systems have been identified over the years.

4.1. Metal nano-constrictions and point contacts

Nano-constrictions and point contacts have been instrumental in the study of quantum corrections to the classical Sharvin resistance [81]. For small contacts, the quantization of the transverse momentum limits the conductance of the contact in a manner analogous to the case of semiconductor/metal-hybrid quantum dots contacts discussed in Section 3.2.2. This allows for a measurement of the properties of individual transport channels. The effect of electron-electron interact between channels has also been measured [82] and explained in terms of Kondo correlations [83]. In contrast to semiconductor heterojunctions, however, the degree of characterization and quantum control is considerably reduced in break-junctions and nano-constrictions.

A frequently occurring feature in such point contacts is a zero-bias anomaly in the differential conductance $G(T, V) = dI/dV\big|_{V=0}$ (here, V is the applied bias voltage across the constriction causing a current I). This anomaly was systematically studied by Ralph and Buhrman [79, 80]. Figure 5(a) provides a sketch of a Cu-based nano-point contact used in the study of [79, 80]. In general, the conductance of the point contact depends on T and V. Surprisingly, however, the conductance difference between $T \neq 0$ and $T = 0$, rescaled by a factor $T^{-1/2}$, only depends on the combination V/T (at sufficiently low T and V). This observation is reproduced in Figure 5(b) from [79, 80]. This scaling plot implies that for the range of V and T over which scaling occurs, the leading T dependence of $G(T, V)$ is $\sim T^{1/2}$ and the leading V dependence is $\sim V^{1/2}$. These results thus appear to be compatible with a 2CK effect and reminiscent of the results shown, *e.g.*, in Figure 3(c). Annealing studies establish that the zero-bias anomaly can be completely eliminated and indicate that the origin of it originates from the structural

disorder in the nano-constriction. Similar results have been obtained using Al-, Ag-, and Pt-based point contacts [79, 80]. More recently, $Al/AlO_x/Sc$ planar tunnel junctions were also shown to feature a zero-bias anomaly with a T and V dependence of $G(T, V)$ that is compatible with an underlying 2CK effect [84].

The fabrication of point contacts and nano-constrictions is generally accompanied by the creation of a considerable amount of structural disorder in the contact. In analogy to the modeling of disorder in metallic glasses and amorphous materials, where such a model captures the T dependence of the specific heat and elastic properties of these systems, the structural disorder is assumed to give rise to double well potentials at the defect locations [85]. Atoms, ions, or electrons, trapped in these double well potentials, mainly occupy the lowest two states in the double well which are thus also known as two-level systems (TLS). A double well potential with its two local minima, separated by a tunneling barrier Δ_0, is shown in Figure 5(c). It was shown by Zawadowski that TLS immersed in a metallic host can be mapped to a 2CK model [37]. This lead to the conjecture that the results reported in Refs. [79, 80] could be a signature of proximity to the 2CK fixed point [86, 87].

Interestingly, the zero-bias anomaly of the point contacts investigated in Refs. [79, 80] show a strong magnetic field (B) dependence. Even at large B field, the dip in the differential conductance is not completely suppressed. The T and V dependence of the resulting electronic state at large B does not concur with expectations for the 2CK nor the single-channel Kondo effect. Not only is the sensitivity to a B field counter intuitive, the lack of a distribution of T_Ks in these highly disordered systems with a presumably broad distribution of parameters like $e/g/\Delta_0$, which characterize the TLSs, is surprising. Moreover, on general grounds, the 2CK model that arises from a TLS does not appear to be in the regime where the singular behavior of the 2CK fixed point is found [88].

4.2. Two-level systems

For a particle localized in a double well potential $V(x)$, one can associate a pseudospin algebra with the lowest two states. The pseudospin degree of freedom is associated with the position of the particle in the double well potential [20]. Assuming for simplicity a symmetric double well potential $V(-x) = V(x)$, the ground state Φ_g will be symmetric, *i.e.*, $\Phi_g(x) = \Phi_g(-x)$ while the first excited state has to be anti-symmetric. Alternatively, one can use the two states which are localized in the left ($|+\rangle$) and right ($|-\rangle$) minimum. These two states form the analog of the spin-up and the spin-down states. If $V(x)$ is not symmetric, $|+\rangle$ and $|-\rangle$ will not be degenerate. This is the analog of a Zeeman splitting h. Spontaneous tunneling between the two states will induce a splitting Δ_0, see Figure 5(c).

Immersed in a metal, the conduction electrons scatter at such a TLS and may

thereby induce assisted tunneling. This is described by an interaction term

$$H_{\text{int}} = \frac{1}{N} \sum_{k,k',\sigma} \Big[\big(2V^0_{k,k'} + V^z_{k,k'} \big(|+\rangle\langle+| - |-\rangle\langle-| \big)$$

$$+ V^x_{k,k'} \big(|+\rangle\langle-| + |-\rangle\langle+| \big) \big) c^\dagger_{k,k',\sigma} c_{k,k',\sigma} \Big], \tag{13}$$

where the hybridization elements $V^i_{k,k'}(i = 0, z, x)$ are overlap integrals of the conduction electron wave function and the local states $|+\rangle$ and $|-\rangle$ and N is the number of k states. It is convenient to introduce the operators $\tau^z_f = |+\rangle\langle+| - |-\rangle\langle-|$ and $\tau^x_f = |+\rangle\langle-| + |-\rangle\langle+|)$. The conduction electron states can now be expanded in terms of spherical waves around the location of the double well potential. Restricting oneself to the lowest terms in the expansion, making use of parity, and transforming into a $|\pm\rangle_c$ basis for the conduction electrons localized at the left or right minimum, one obtains [37, 89, 90]

$$H_{\text{2CK}} = \sum_{k,\alpha_\pm,\sigma} \varepsilon_k c^\dagger_{k,\alpha,\sigma} c_{k,\alpha,\sigma} + \Delta_0 \tau^x_f$$

$$+ \sum_{\alpha,\beta,\sigma} \Big(V^z \tau^z_f \tau^z_c \big|_{\alpha,\beta} + V^x \tau^x_f \tau^x_c \big|_{\alpha,\beta} \Big) \sum_{k,k'} \frac{1}{N} c^\dagger_{k,\alpha,\sigma} c_{k,\beta,\sigma} \tag{14}$$

where τ^i_c $(i = x, z)$ are Pauli matrices in the $|\pm\rangle_c$ basis and the term $\sim V^0_{k,k'}$ has been dropped, so that Equation (14) is just the 2CK Hamiltonian. H_{2CK} is diagonal in the spin channel. Thus, the electron spin provides two degenerate, independent screening channels which are expected to overscreen the local pseudospin. However, as pointed out by Moustakas, the term $\sim V^0_{k,k'}$ contains in general a direct tunneling term $\sum_{k,k'} c^\dagger_{k,+,\sigma} c_{k',-,\sigma}$ [91]. Such a term is relevant at the 2CK fixed point and would drive the system away from it. This has lead to the question how the presence of higher excited states will modify Equation (14) [92]. This question was finally settled in Refs. [93, 94] by considering the action of a heavy particle of mass M in a general double well potential $V(x)$ interacting with conduction electrons. After bosonizing the action and integrating out the conduction electrons, the authors of [94] were able to cast the action into the form of a one-dimensional Coulomb gas of $+$ and $-$ charges (*i.e.* kinks and anti-kinks) describing the tunneling events between the classical trajectories which are solutions of $M d^2/d\tau^2 = dV/dx$. As discussed in Section 2.1, the Kondo problem has a very similar representation of its actions with which the results of Ref.[94] can be compared. This lead to the conclusion that the effective (renormalized) $\tilde{\Delta}_0$ will always be much larger than the dynamically generated T_K of the problem, making it impossible to enter the scaling regime of the 2CK fixed point. Therefore, TLS do not appear to be a likely route towards observation of the 2CK fixed effect [94].

If the generation of direct tunneling terms could be avoided, a different conclusion might be reached. This insight led Moustakas and Fisher to consider defects that tunnel with a triangular symmetry. In this case, group theory ensures that a double degenerate level has to exist in the spectrum. A possible issue with this proposal is that in general higher dimensional irreducible representation commonly only occur for excited states, not the ground state [91].

4.3. Electron-electron interaction and weak localization corrections

The search for realizations of the 2CK impurity effect in generic quantum materials confronts us with an additional complication. In order to measure the effect of dynamic scattering centers in a solid, a sufficiently large number is required to detect signatures in thermodynamic and transport properties. Yet, the concentration should be low enough so that one can safely ignore correlation effects between these quantum impurities. This places the system in the dilute limit. Supposing that these impurities may not give rise to 2CK behavior but, instead, only act as simple potential scatterer. This inevitably affects the mean free path of the conduction electrons of the host metal, l_e, and places the system into the domain of weak disorder, defined as the regime where the Fermi wavelength λ_F is much shorter than l_e. This results in a collision time $\tau_e \sim l_e/v_F$ with v_F being the Fermi velocity. At time scales much larger than τ_e, the electron motion is diffusive with a diffusion constant given by $\mathcal{D} = v_F l_e/d$, where d is the space dimension [95, 96]. A comprehensive review of experiments on electron dephasing has been given by Lin and Bird [97].

Due to the diffusive motion of the electrons in a weakly disordered metal, which is slower than in the clean limit, the effect of the electron-electron interaction is enhanced. As a result, the quasi-particle lifetime is modified. Fluctuations in the electron density due to electron-electron interaction affect the energy levels near the Fermi and therefore the density of states $N(E)$ near E_F. As a consequence, the electron-electron interaction in the disordered metal will result in a decrease of $N(E \approx E_F)$ from its clean limit. This is known as the Altshuler-Aronov anomaly [98]. At the linear response level, transport properties can be obtained from $N(E)$, so that the Altshuler-Aronov anomaly also leads to a dimension-dependent correction to the conductance δG, which is given by [96]

$$\delta G(T) \sim -u \begin{cases} \dfrac{\sqrt{\hbar\mathcal{D}/T}}{L}, & d = 1 & \text{(15a)} \\[2ex] \ln\left(\dfrac{\sqrt{\hbar\mathcal{D}/T}}{l_e}\right), & d = 2 & \text{(15b)} \\[2ex] \dfrac{L}{l_e} - \dfrac{\sqrt{T}L}{\sqrt{\hbar\mathcal{D}}}, & d = 3, & \text{(15c)} \end{cases}$$

where u is a dimensionless parameter that measures the interaction strength and L is the linear dimension of the system. In $d = 2$, the correction has a logarithmic temperature dependence. In $d = 3$, however, it displays a square-root dependence in T, just like the T dependence expected for the 2CK effect! Although, the Altshuler-Aronov anomaly is a small correction, it appears generically without the need of fine-tuning. Its amplitude is fully determined by a few bulk properties [95, 96, 97, 98]. In order to consider if a two-dimensional system of finite width W should be treated as a two- or three-dimensional system, one has to compare τ_ϕ to $W^2/\mathcal{D}$, *i.e.*, the time it takes the electron to diffuse a distance W. If $\tau_\phi \gg W^2/\mathcal{D}$, we have $d = 2$. In the opposite case, the system is effectively three-dimensional. In an anisotropic system and for weak disorder, it turns out that all results hold true in terms of an anisotropic diffusion coefficient [99].

The perhaps most likely route to 2CK behavior in real materials will rely on a pseudospin degree of freedom for the Kondo exchange scattering. The spin degeneracy of the conduction electrons, ensured by Kramers' theorem for time-reversal invariant systems, would then give rise to two independent screening channels and induce overscreening. The spin degeneracy remains unaffected for magnetic field strengths which are tiny compared to the half-bandwidth of the conduction electrons. Thus, a clear understanding of the magnetoresistance of a disordered metal may help to distinguish between the resistivity signatures in a magnetic field of the 2CK fixed point and those caused by the electron-electron interaction due to disorder [100].

In addition to the Altshuler-Aronov anomaly, the conductivity is reduced by a quantum effect that originates from the interference of time-reversed paths that can be transversed within the coherence time τ_ϕ. This contribution is known as the weak localization correction. Its overall structure resembles that of the Altshuler-Aronov correction. While the weak localization correction is affected by the presence of a magnetic field, the Altshuler-Aronov correction is insensitive to it. In a weakly, three-dimensional disordered metal, the conductivity correction in a magnetic field is thus given by [96]

$$\delta\sigma(T,B) = \frac{1.3e^2}{4\pi^2\hbar}\left(\frac{4}{3} - \frac{3}{2}\tilde{F}\right)\sqrt{\frac{T}{\mathcal{D}}} - \frac{e^2}{\hbar}\frac{\tilde{F}}{4\pi^2}\sqrt{\frac{T}{2\mathcal{D}}}\tilde{g}(h), \tag{16}$$

where the function $\tilde{g}$ depends on the reduced field $h = g\mu_B B/k_B T$ (μ_B is the Bohr magneton and k_B is the Boltzmann constant). It has the asymptotics $\tilde{g}(h) \sim h^2$ for $h \ll 1$ and $\tilde{g}(h) \sim \sqrt{h}$ for $h \gg 1$. Its explicit form $\tilde{g}$ can be found in Ref. [96], which gives a comprehensive review of transport in disordered metals. $\tilde{F}$ is the so-called screening factor. For strong screening of the electron-electron interaction, $\tilde{F}$ approaches 0. A field independent conductivity correction as in a non-magnetic 2CK impurity is expected for $\tilde{F} = 0$. In general, $\tilde{F}$ is difficult to calculate accurately[95].

4.4. Ferromagnetic L1$_0$-Mn(Al,Ga) films

An intriguing resistivity increase observed in MnAl has been reported in Ref. [101] and related materials [102]. MnAl is of technological importance due to its interesting ferromagnetic properties. It has a large magnetic moment of 2.4 μ_B per formula unit and a Curie temperature of $T_C = 650$K [103]. These highly disordered MnAl alloys possess the L1$_0$ structure and can display a pronounced $T^{1/2}$-increase in their low T $\rho(T)$. This $T^{1/2}$-increase has been observed epitaxially grown L1$_0$ films [101, 102], see Figure 6(a) and (b). The growth conditions result in considerable strain in the films due to lattice mismatch with the substrate and generate disorder. The temperature of the substrate during growth, T_S, controls the amount of this structural disorder. The measured dependence of $\rho(T)$ on T_S is reproduced in Figure 6(a) and points to the influence of disorder in the film. Similar results have also been reported for ferromagnetic L1$_0$-MnGa films [102].

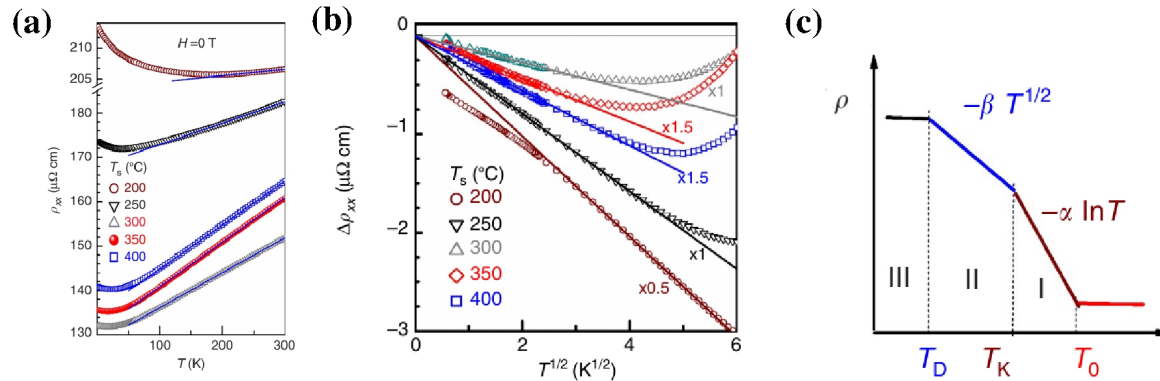An orbital 2CK effect has been invoked by Zhu et al. to explain the T dependence

Figure 6. Transport in epitaxially grown $L1_0$ MnAl films with the $L1_0$ structure. (a) Resistivity $\rho(T)$ vs. temperature for different T_S, where T_S is the substrate temperature during the growth of the film. The data for $T_S = 200K$ and $T_S = 250K$ display a marked increase in $\rho(T)$ for $T < 50K$. (b) $\Delta\rho_{xx}(T)$ vs. $T^{1/2}$, where $\Delta\rho_{xx}(T)$ is the difference of the resistivity $\rho(T)$ and a background contribution defined through a best fit procedure. (c) $\rho(T)$ is argued to display three different regimes: in (I) $\rho(T) \sim \log(T)$, (II) is a $\sqrt{T}$ behavior and (III) is a crossover to a Fermi liquid regime where $\rho(T) \sim T^2$. (Data taken from [101]).

of $\rho(T)$ [101]. Zhu et al. point out that three different transport regimes are observed in the T behavior of $\rho(T)$: At high T, a logarithmic-in-T behavior is observed, followed by a $\rho(T) \sim T^{1/2}$ regime towards lower T. Lowering T even further, one observes a crossover in $\rho(T)$ to a T^2 dependence [101]. This is schematically portrayed in Figure 6(c). According to the authors of Ref. [101] each of the three transport regimes can be identified with a transport regime of the non-magnetic 2CK problem. The $T^{1/2}$ regime of $\rho(T)$ is reproduced in Figure 6(b). Interestingly, only the data for $T_S = 200°$ seem to show a deviation from the $T^{1/2}$ towards lower T.

The origin of the conjectured 2CK physics in these $L1_0$-MnAl films would be the Kondo scattering generated by conduction electrons tunneling off either atoms, atom groups or electrons in defect-generated double-well potentials. As a result, one obtains two-level systems coupled to conduction electrons and hence a 2CK model realization [101].

A number of observations are noteworthy. As discussed in Section (4.2), induced tunneling at TLSs does not offer a viable route to the 2CK effect. Moreover, assuming that indeed anisotropic 2CK impurities exist in the films, no logarithmic-in-T behavior in $\rho(T)$ at high T is expected for the model of Equation (14) [104].

The general difficulties in realizing the 2CK fixed point are related to the high demand on channel symmetry. In the proposed model, Equation (14), the two screening channels are provided by the two spin projections of the conduction bands in $L1_0$-MnAl. On the other hand, time-reversal invariance in $L1_0$-MnAl is broken due to the ferromagnetism and the exchange splitting is large, i.e., of the order of $2eV$. Unfortunately, Ref. [101, 102] does not explain how a 2CK effect could possibly survive in such a strong exchange field. For comparison, placing a spin-1/2 moment in an

antiferromagnet, where the average moment vanishes, destroys the one-channel Kondo effect [105]. It thus seems unlikely that a 2CK effect, either magnetic or orbital, could form deep in a ferromagnetic phase.

The authors in [101] also report a weak negative magnetoresistance over the T range from 2K to 300K that is displaying a $\sqrt{B}$ dependence on the applied magnetic field B. While it is stated that this dependence is unlikely related to the T dependence of $\rho(T)$ in the supposed 2CK regime, the precise origin of the negative magnetoresistance remains, according to Ref. [101], unclear.

From the discussion in the previous subsection it follows, however, that weak localization corrections to $\rho(T)$ are compatible with a $B^{1/2}$ dependence.

In Figure 6(a), the data of [101] are reproduced. As one can see, in the film grown on a surface at $T_S = 200°$C shows a pronounced increase of $\rho(T)$ starting at around 150K. This particular sample appears to be located close to a metal-insulator transition and may not be well described by the theory for weakly disordered metals. Only the data for $T_S = 200°$, however, seem to show a deviation from the $T^{1/2}$ towards lower T. Similar arguments may apply to a weaker degree to the film grown at $T_S = 250°$C. The films grown at $T_S = 300°$C, $350°$C, and $400°$C on the other hand appear to be in the weakly disordered regime and their $\rho(T)$ seems to be explainable in terms of the Altshuler-Aronov correction.

It therefore seems conceivable that the reported behavior for epitaxially grown ferromagnetic $L1_0$-MnAl films is compatible with expectations for electron-electron interaction effects in weakly disordered metals. It is most likely not caused by disorder-driven orbital 2CK physics. A similar conclusion has recently been reached by Zhu and Zhao [106].

4.5. Ferrimagnetic LaNiO₃-CoFe₂O₄ composites

Ferrimagnetic $LaNiO_3$-$CoFe_2O_4$ composites have been investigated in Ref. [107]. These composites have the general composition $(1 - x)LaNiO_3 + xCoFe_2O_4$ and are ferrimagnetic as a result of the ferromagnetism of $LaNiO_3$ which forms below $T_C = 520°$K. Thermodynamic and transport properties for a range of x including $x = 0, 0.10, 0.15, 0.20, 0.25$ are reported in Ref. [107].

In Figure 7, the transport data for $x = 0.10$ are reproduced. Figure 7(a) depicts $\rho(T)$ over the full measured range from 10K to 300K. In an applied magnetic field the data show an upturn as T is lowered starting at around 30K. In Figure 7(b) this upturn is analyzed in terms of an $\log(T)$ dependence while in Figure 7(c) $\rho(T)$ is plotted against $T^{1/2}$. Both, Figures 7(b) and (c), display a linear dependence of the data. In contrast, for pure $LaNiO_3$, no $\rho(T)$ anomalies are observed. From the magnetic field dependence, *i.e.*, a negative magnetoresistance, the authors conclude that for $x = 0.10$ $LaNiO_3$-$CoFe_2O_4$ composites displays a spin-1/2 (magnetic) one-channel Kondo effect.

For $x = 0.15$, an overall similar behavior of $\rho(T)$ to that of $x = 0.1$ is found [107]. This behavior can be fitted to a logarithmic temperature dependence at higher T
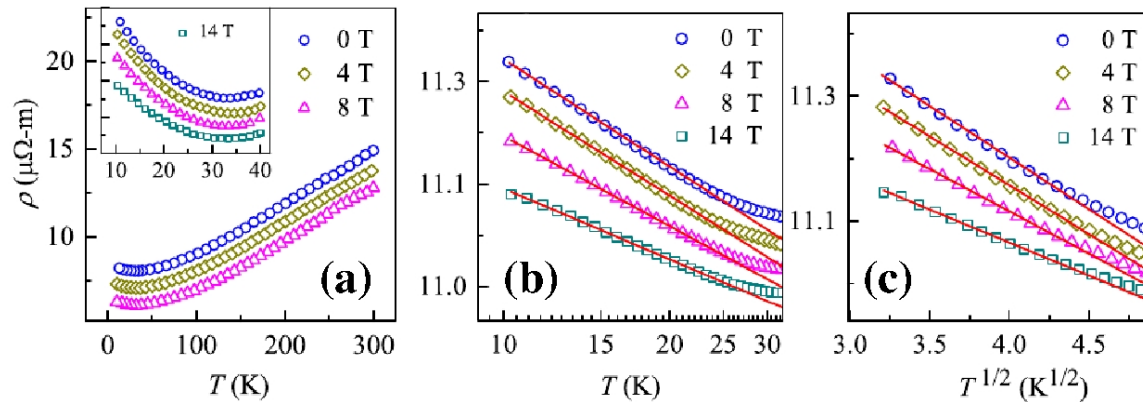
Figure 7. Transport properties of ferrimagnetic composites with 10% $CoFe_2O_4$. (a) Resistivity $\rho(T)$ vs. temperature T for a range of magnetic fields. The inset zooms in on the low T upturn. (b) $\rho(T)$ in a semi-log plot. The straight lines are logarithmic in T. The amplitudes have been obtained from fits to the data. (c) Same data as in (b) plotted against $T^{1/2}$. The straight lines are square-root in T. The amplitudes have been obtained from fits to the data. The magnetic field dependent data in (a), (b), and (c) have been shifted vertically for clarity. (Data taken from [107])

followed by a $\sqrt{T}$ increase upon cooling. The magnetic field independence of both the $\ln(T)$ and $\sqrt{T}$ behavior of $\rho(T)$ is interpreted as evidence for an orbital 2CK effect due to structural disorder. From a fit to the $\ln(T)$ and $\sqrt{T}$ behavior, the authors of Ref. [107] infer a $T_K \approx 18.5$K.

The specific heat data for $x = 0.1$ and $x = 0.15$ show a linear-in-T dependence down to ~ 20K. Below ~ 20K, deviations occur which are attributed to the presence of two-level systems with a corresponding distribution of energy levels [107].

Again, a few cautionary remarks are in order regarding the interpretation of the observed resistivity anomalies in terms of magnetic single-channel Kondo physics for $x = 0.10$ and orbital 2CK physics for $x = 0.15$. By and large, these concerns are similar to the ones raised in subsection 4.4. Specifically, (1) two-level systems are an unlikely source of orbital 2CK physics. (2) for an anisotropic 2CK model like the one invoked by the authors to explain the $x = 0.15$ data, no $\ln(T)$ behavior in $\rho(T)$ above the $\sqrt{T}$ regime is expected [104]. (3) Due to the non-vanishing ordered moment in the The $LaNiO_3$-$CoFe_2O_4$ composites, neither magnetic single-channel Kondo (for $x = 0.10$) nor non-magnetic 2CK physics (for $x = 0.15$ is expected. Unfortunately, Ref. [107] does not provide any explanation or proposed model for how structural disorder could give rise to local magnetic moments at $x = 0.1$ while at $x = 0.15$ these local magnetic moments have been replaced by non-magnetic dynamic scatterers that drive an orbital 2CK effect. All this would have to happen in the dilute limit, where inter-impurity effects can be neglected and in the presence of the underlying magnetic order.

If the interpretation of Ref. [107] is correct, $\rho(T)$ for $x = 0.10$ is expected to develop Fermi liquid behavior well below T_K. Since $T_K \approx 18$K, $\rho(T)$ measurements down to 1K should not only be helpful in extending the fitting range in order to distinguish between

a logarithmic-in-T and a square-root-in$T$ dependence. They should also be able to indicate if a Kondo-screened Fermi liquid state forms for $x = 0.10$. Alternatively, the observed behavior of $\rho(T)$ in LaNiO$_3$-CoFe$_2$O$_4$ composites may just be a reflection of electron-electron interaction effects that generically form in weakly disordered metals.

4.6. Arsenic vacancies in the PbFCl structure type

Several As-based metallic systems possessing the PbFCl structure, a substitution variant of the Fe$_2$As type, *e.g.*, ThAsSe or HfAs$_{1.7}$Se$_{0.2}$, display a magnetic-field independent low T resistivity anomaly, $\rho(T) = \rho_0 - |A|\sqrt{T}$, where $\rho_0 = \rho(T = 0)$ denotes the residual resistivity [108, 109]. In order to address the origin of this anomaly, the authors of Ref. [110] identified two homologues with largely similar physical properties and combined precise physical measurements with chemical and structural analyses performed on the same single crystal. As a result, the authors reached the conclusion that the transport anomaly in ZrAs$_{1.58}$Se$_{0.39}$ has to be generated by a 2CK effect which is driven by As vacancies.

The homologue to ZrAs$_{1.58}$Se$_{0.39}$ used for comparison in Ref. [110] is ZrP$_{1.54}$S$_{0.46}$. Both pnictide-chalcogenides condense in the tetragonal ($P4/nmm$) PbFCl structure which is shown in Figure 8(a). This crystal structure consists of square-planar 4^4 nets stacked along the [001] direction. A fundamental difference of arsenide selenide compared to other pnictide-chalcogenides is that the homogeneity range of the ternary system Zr-As-Se is located to the right of the tie-line ZrAs$_2$–ZrSe$_2$ on the As depleted side, see Figure 8(b). A careful structural analysis conducted by the authors of Ref. [110] reveals that vacancies only occur within the As layers of ZrAs$_{1.58}$Se$_{0.39}$, denoted Pn$_{2a}$ in Figure 8(a). In contrast, in the homologue ZrP$_{1.54}$S$_{0.46}$, located on the tie-line, the Pn$_{2a}$ layer is completely filled.

As it turns out, a replacement of As and Se by P and S, does not substantially alter basic physical properties, such as the overall behavior magnitude of $\rho(T)$ and the specific heat. This suggests that the Altshuler-Aronov correction in both homologues should be similar. This conclusion is based on the following observation: The comparatively small Altshuler-Aronov correction to $\rho(T)$ depends on the phase relaxation and electron-electron collision times. These, in turn, are determined by the diffusion constant, $\mathcal{D}$, and the density of states at the Fermi energy, N_0, and can be estimated from underlying bulk properties [96, 98, 111].

Interestingly, the superconducting properties of both homologues are noticeably different from each other: While ZrP$_{1.54}$S$_{0.46}$ undergoes a superconducting transition at $T_C \approx 3.9$K, the superconductivity onset temperature in ZrAs$_{1.58}$Se$_{0.39}$ is reduced down to $T_C \approx 0.14$K.

The $\rho(T)$ anomaly of ZrAs$_{1.58}$Se$_{0.39}$ that sets in around 15K and, for $B = 0$, is interrupted by the superconducting transition at $T_C \approx 0.14$K, turns out to be completely field-independent, as shown in Figure 8(b). Shown are the results for two samples of ZrAs$_{1.58}$Se$_{0.39}$, with similar elastic relaxation rates. These were cut from the same crystal

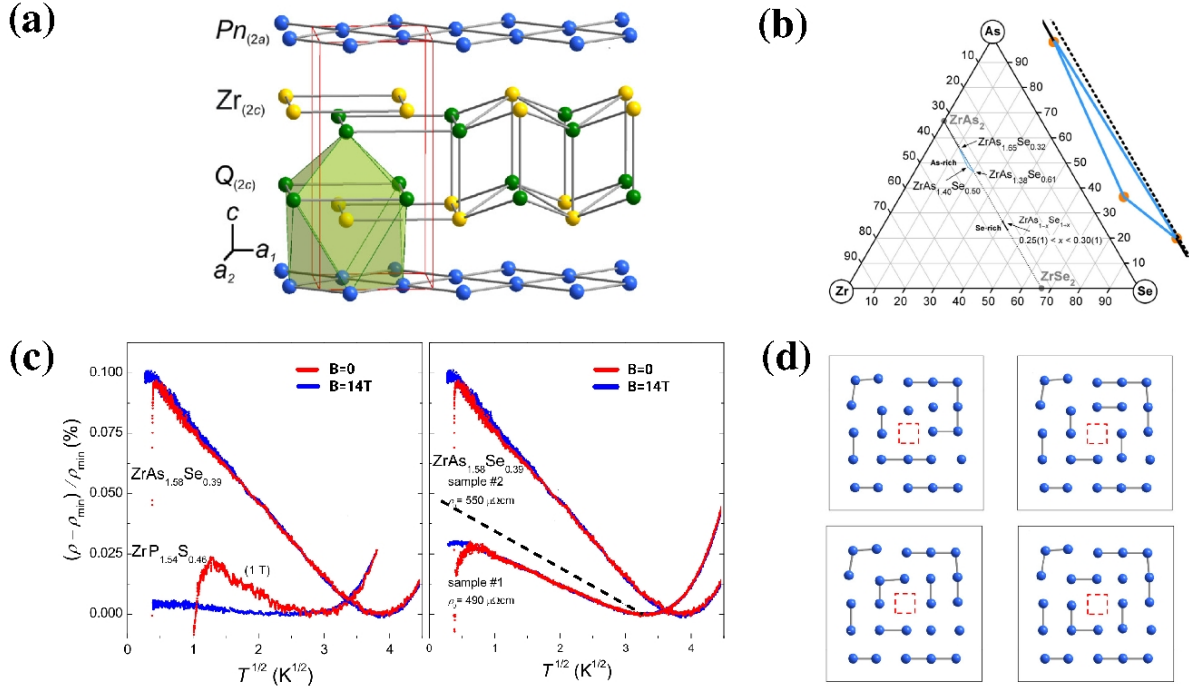**Figure 8.** 2CK effect in $\mathrm{ZrAs_{1.58}Se_{0.39}}$: (a) The PbFCl structure of ziconium pnictide chalcogenides. The $\mathrm{Pn_{2a}}$ layer of $\mathrm{ZrAs_{1.58}Se_{0.39}}$ contains As vacancies but is completely filled in the case of $\mathrm{ZrP_{1.54}S_{0.46}}$. (b) The ternary system Zr-As-Se at 1223K. The very narrow homogeneity range of the ternary phase is enlarged on the right hand side. The dashed line is the tie-line between the binary compounds $\mathrm{ZrAs_2}$ and $\mathrm{ZrSe_2}$. The homogeneity range of the arsenide selenide, is shifted from the tie-line $\mathrm{ZrAs_2}$–$\mathrm{ZrSe_2}$ and forms a triangle between the chemical compositions $\mathrm{ZrAs_{1.65}Se_{0.32}}$, $\mathrm{ZrAs_{1.38}Se_{0.61}}$ and $\mathrm{ZrAs_{1.40}Se_{0.50}}$. (c) Left: $\rho(T)$ vs. T for $\mathrm{ZrAs_{1.58}Se_{0.39}}$ and $\mathrm{ZrP_{1.54}S_{0.46}}$ in zero field ($B=0$) and at $B=14T$. Right: Data of two different samples of $\mathrm{ZrAs_{1.58}Se_{0.39}}$, #1 and #2, are shown. The dotted line is the expected amplitude for sample #2 of a hypothetical Altshuler-ARonov correction wit $\tilde{F}=0$ obtained by fitting $\mathcal{D}$ from sample #1. (d) Different possible arrangements of oligomers due to As vacancies in the Pn(2a) layer shown in (a). The lower two panels show two configurations that are related by a $\mathrm{C_{4\nu}}$ operation. (Data taken from [110]).

which possesses a homogeneous distribution of Zn and Se and only small variations of As [110].

In Figure 8(c) $(\rho - \rho_{\min})/\rho_{\min}$ vs. $T^{1/2}$ is shown for both homologues; in zero field and at $B = 14T$. In contrast to $\mathrm{ZrAs_{1.58}Se_{0.39}}$, $\rho(T)$ in $\mathrm{ZrP_{1.54}S_{0.46}}$ does not show a pronounced $T^{1/2}$ behavior and an applied B-field suppresses the signal almost completely. This suggests that the Altshuler-Aronov anomaly and the effect of the electron-electron interaction is negligible in this compound and by virtue of the similarity of the two homologues, the same should hold true for $\mathrm{ZrAs_{1.58}Se_{0.39}}$.

This is further corroborated by the following consideration. Assuming that the data in Figure 8(c) for sample #1 of $\mathrm{ZrAs_{1.58}Se_{0.39}}$ were a consequence of the Altshuler-Aronov correction with $\tilde{F} = 0$, so that the $T^{1/2}$ amplitude becomes B-field independent, see Equation (16), the corresponding amplitude for sample #2 under this assumption

can be inferred. The dashed line in Figure 8(c) is the resulting magnitude of this hypothetical Altshuler-Aronov $-|A|T^{1/2}$ correction to $\rho(T)$ for sample #2. It is thus concluded that the origin of the anomalous $-|A|T^{1/2}$ in the low T $\rho(T)$ of $ZrAs_{1.58}Se_{0.39}$ is caused by a non-magnetic 2CK effect which is driven by As vacancies [110, 112].

For square nets in compounds possessing the PbFCl structure it is known that vacancies will result in a Jahn-Teller distortion which will be accompanied by the formation of As oligomers [113]. Different possible Jahn-Teller distortions and oligomer configurations are shown in Figure 8(d). The lower two panels show configurations that are related by a $C_{4\nu}$ operation and thus have identical energies as a vacancy in the square net preserves the $C_{4\nu}$ symmetry. A pseudospin representation associated with the Jahn-Teller distortion is then used to write the conduction electron induced transitions between different Jahn-Teller distortions related by the $C_{4\nu}$ symmetry as an effective Kondo exchange term between the local pseudospin and that of the conduction electrons. This results in a 2CK model where the conduction electron spin labels degenerate screening channels [91, 110, 114, 115].

One possible issue with this proposed scenario is that the pseudospin doublet is in general not the ground state of the local system. This, however, may change when the coupling of the doublet to the conduction electrons is considered [116]. In fact, numerical renormalization group studies suggest that the doublet energy can get renormalized below the singlet in a wide parameter regime[117]. The conclusion that $ZrAs_{1.58}Se_{0.39}$ displays a 2CK effect is further corroborated by the suppressed T_C, as compared to that of $ZrP_{1.54}S_{0.46}$, which points to the presence of efficient Cooper pair breakers [118].

The interpretation for $ZrAs_{1.58}Se_{0.39}$ in terms of a 2CK effect has recently been called into question in Refs. [119, 120]; see also [112]. The author of [119, 120] points out that a proper estimate of the electron-electron interaction has to take into account the anisotropy of $\rho(T)$ in the basal plane (ρ_a) and perpendicular to it (ρ_c). This is a valid argument and some anisotropy is expected since both pnictide-chalcogenides are layered compounds. Part of the ongoing discussion is about the correct value of this transport anisotropy. Due to sample geometry, ρ_a cannot be measured reliably up to the necessary precision required for the tiny relative amplitude of the anomaly (see Figure 8(c)). A consistent explanation should, however, also address the apparent absence of a noticeable Altshuler-Aronov correction in $ZrP_{1.54}S_{0.46}$, given that basic properties are similar to $ZrAs_{1.58}Se_{0.39}$, which should be enough to determine the amplitude of the Altshuler-Aronov correction through Equation (15c).

As superconductivity cuts off the $-|A|T^{1/2}$ anomaly, no deviations from the square-root behavior in $B = 0$ are observable, which would be a clear signal in favor of the 2CK interpretation. Therefore, at present, it seems unclear as to what is the underlying cause of the $\rho(T)$ anomaly observed in $ZrAs_{1.58}Se_{0.39}$.

(a)

(b)

d_{xz}

E

$d_{x^2-y^2}$ d_{z^2}

d_{xy} d_{xz} d_{yz}

free ion

CEF splitting in a
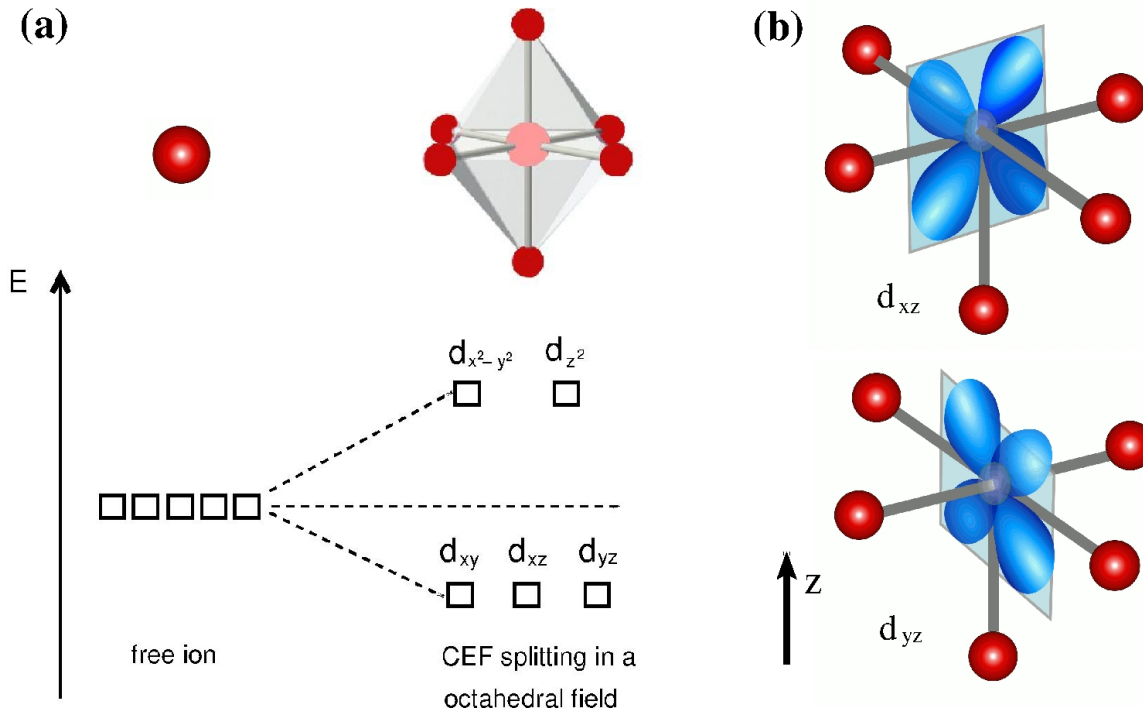octahedral field

Z

d_{yz}

Figure 9. (a) The d-electron levels of a free atom or ion are degenerate due to the isotropy of free space. In a crystalline environment, this isotropy is broken down to the point group of the crystal. In an octahedral crystal electric field this symmetry reduction forces the five d-orbitals to split up into two set of degenerate levels with threefold and twofold degeneracy. (b) If the octahedral symmetry is further reduced, *e.g.*, due to a nearby vacancy, further degeneracy lifting will occur. In the case depicted here, a C_{4v} symmetry is still present, even though an ion in the surrounding octahedron was removed. Group symmetry implies that a double-degeneracy, associated with the two-dimensional irreducible representation of the C_{4v} group, still exists. It is easy to see, that this remaining degeneracy in the case depicted here is related to the d_{xz} and d_{yz} orbitals.

4.7. Vacancies in crystals with octahedral symmetry

The ongoing discussion of what causes the low T transport anomaly in $ZrAs_{1.58}Se_{0.39}$ not only brings out the difficulties involved in disentangling different possible causes for $\sqrt{T}$ contribution to $\rho(T)$ at low T, it also indicates that symmetry considerations are essential in avoiding the difficulties associated with the TLS's route towards the 2CK fixed point.

In the context of lanthanide and actinide intermetallics, it has long been speculated that the unusual metallic behavior displayed by some of these compounds might be explained in terms of a 2CK lattice [20, 121, 122]. One of the earliest suggestions along this line was put forth by D. Cox, who suggested that tetravalent Uranium-based heavy-electron metals like UBe_{13} may develop a quadrupolar Kondo effect due to orbital degrees of freedom of the $5f$ shell of the Uranium ions [123].

One of the common symmetries in crystal structures is related to fourfold rotations

as well as reflections and leads to the $C_{4\nu}$ point group. This group is non-abelian and possesses a two-dimensional irreducible representation. As a result, the excitation spectrum of a quantum object placed in a fourfold potential will possess an orbital degeneracy. We refer to the corresponding basis functions as $|\Gamma_{2\text{dim}}+\rangle$ and $|\Gamma_{2\text{dim}}-\rangle$ and use $|\Gamma_{2\text{dim}}i\rangle$ ($i = \pm$) as components of a pseudospin-1/2 variable. The Great Orthogonality Theorem ensures that the conduction electron wavefunction at the site of the quantum impurity, $|\Psi\rangle$, can be decomposed in terms of the basis functions of the irreducible representations as

$$|\Psi\rangle = \sum_{\Gamma_{n'}} \sum_{j'} f_{j'}^{(\Gamma_{n'})} |\Gamma_{n'} j'\rangle , \tag{17}$$

where $|\Gamma_m i\rangle$ denotes the ith basis function of the mth irreducible representation. Since $\langle \Gamma_n j | \Gamma_m i \rangle = \delta_{m,n} \delta_{i,j}$, the pseudospin associated with the two-dimensional representation is locally conserved. This will ensure the absence of terms that otherwise would be relevant at the 2CK fixed point and lead to a pseudospin-exchange interaction. The real spin of the conduction electrons acts as a dummy index which labels different, degenerate screening channels.

Expanding the conduction electron states around the quantum impurity yields

$$H = H_{\text{loc}} + Q_1 \sum_{\sigma} (d_+^\dagger d_+ - d_-^\dagger d_-)(c_{+,\sigma}^\dagger c_{+,\sigma} - c_{-,\sigma}^\dagger c_{-,\sigma}) \tag{18}$$
$$+ \Delta_1 \sum_{\sigma} (d_+^\dagger d_- c_{-,\sigma}^\dagger c_{+,\sigma} + d_-^\dagger d_+ c_{+,\sigma}^\dagger c_{-,\sigma}) + H_{\text{add}},$$

where H_{loc} contains the local part of the dynamic defect, $d_\pm^\dagger$ creates an electron in the basis state $|\Gamma_{2\text{dim}}\pm\rangle$, $c_{\pm,\sigma}^\dagger$ is the local conduction electron creation operator projected onto the basis states of the set of irreducible representations of the local symmetry. The term proportional to Q_1 describes the coupling of the z-component of the pseudospins whereas Δ_1 is the (pseudo-) spin-flip component responsible for Kondo-scattering processes. H_{add} contains all additional terms of the Hamiltonian. As the conduction electron spin degree of freedom σ only enters as an overall summation index and the degeneracy in σ is protected by time-reversal symmetry, the model is equivalent to the 2CK model. Such a scenario could be realized in d-electron systems with octahedral symmetry. In such a material, the octahedral field induces a splitting of the five-fold degenerate state into t_{2g} and e_g orbitals, see Figure 9(a). This symmetry can be further reduced near lattice defects. For vacancies like the one shown in Figure 9(b) the symmetry is reduced to a $C_{4\nu}$ symmetry (with an axis through the central ion and the vacancy). It is intuitively clear, that in this situation the orbitals d_{xz} and d_{yz} have to be degenerate. These two orbitals form the local pseudospin degree of freedom.

The local energetics has to be such, that the effective model of Equation (18) is placed in its Kondo regime. A realization of this model is expected to display a B-field independent low T $\rho(T) \sim T^{1/2}$ anomaly which should be sensitivity to strain. The effect of strain in this scenario would be similar to that of magnetic fields on a magnetic Kondo impurity as it will tend to lift the degeneracy of d_{xz} and d_{yz}. The observation of

2CK and one-channel orbital Kondo physics in transition metal rutile nanowires in line with such a scenario has recently been reported by S.-S. Yeh et al. [124].

4.8. Single-ion effects and disorder in 4f electron systems

Kondo lattice systems frequently occur in lanthanide-based intermetallics involving Cerium or Ytterbium and have also been invoked to explain the low-T physics of certain actinide-based intermetallics containing Uranium ions. In these systems, a local moment is associated with the $4f$ or $5f$ shell.

This raises the question if 2CK lattices in d or f electron systems could form, generalizing the arguments presented in Section 4.7. In contrast to a standard Kondo lattice, where the conduction electron band is diagonal in the Kondo-active degree of freedom, *e.g.*, the electron spin projection, the Kondo exchange interaction in terms of a pseudospin exchange interaction relies on an expansion of the conduction electrons at the site of the localized pseudospin degree of freedom. This expansion in terms of basis functions is in general only locally valid. This should affect the form of the pseudospin analog of the RKKY interaction, except for the special situations where the conduction electrons would carry the basis function label as a good quantum number. This not withstanding, 2CK lattices have been the subject of a number of theoretical investigations [21, 125, 126].

As far as UBe$_{13}$ is concerned, the existence of a quadrupolar Kondo effect [123] could not be confirmed so far. A possible reason might be that in contrast to their $4f$ counterparts, $5f$ orbitals are substantially less localized. As a result, crystal-electric fields are less-well defined.

Dilution studies as in Ref. [121] to bring out single-ion 2CK physics that may exist in the dense lattice case encounter yet another difficulty. In Kondo lattices with disorder in the Kondo exchange coupling, it has been shown that a distribution of Kondo temperatures $P[T_K]$ can lead to an apparent non-Fermi liquid behavior with a strong resemblance to the strange metal phase [127, 128, 129]. As Miranda and co-workers demonstrated, the main ingredient is a $P[T_K]$ that behaves as $P[T_K] = A_0 + A_1 T_K + A_2 T_K^2 + \dots$ for T_K smaller than some cutoff Λ. In such a situation, one expects for the distribution averaged γ coefficient of the specific heat [127]

$$\langle C/T \rangle = \int_T^\Lambda dT_K \, P[T_K] \frac{C_0}{T_K} \sim A_0 C_0 \ln\left(\Lambda/T\right) \qquad (19)$$

for T well below Λ. It can also be shown that $\rho(T) = \rho_0 - aT$ [127]. In certain materials, *e.g.*, Ge-based filled skutterudites, it has been explicitly demonstrated that Kondo disorder does indeed lead to a non-Fermi liquid phase at the border of magnetism [130]. This prompts the question of how to distinguish between disorder- and interaction-driven non-Fermi liquid phases beyond beyond leading powerlaw behavior in C/T and $\rho(T)$; two bulk quantities that are comparatively easy to measure.

5. Conclusions and Outlook

Motivated by the current interest in singular Fermi liquids and strange metal phases, I reviewed a range of proposed realizations of the 2CK effect as a route to non-Fermi liquid behavior. Despite the fact that two-channel Kondo physics is conceptually among the simplest possible ways of critically destroying a Fermi liquid, its physical realization rests on a carefully balanced competition between degenerate screening channels. In engineered semiconductor and metal-hybrid heterostructures which can be meticulously tuned, this frustrated situation between the screening channels can be ensured for an intermediate range in energy and temperature. These systems with their high degree of characterization and control therefore form at present the most clear and perhaps only commonly accepted realizations of the two-channel Kondo effect. The resulting characteristic energy scale, *i.e.*, T_K of these systems is, however, comparatively small.

In real quantum materials the situation is more complex when it comes to identifying a two-channel Kondo effect. A Fermi liquid is unstable against disorder but weak disorder in the metallic host seems unavoidable when attempting to create two-channel Kondo impurities. Electron-electron interaction effects in the metal then give rise to the Altshuler-Aronov correction which seems to explain many of the proposed candidate materials for two-channel Kondo behavior.

A convincing demonstration of two-channel Kondo criticality in a generic quantum material would require to establish non-Fermi liquid scaling with the anticipated powerlaw exponents over an extended range in temperature and possibly energy. Moreover, the host material should only be weakly correlated and not located in proximity to a phase transition. In order to avoid the emergence of relevant perturbations, the two-channel scattering centers should be symmetry-protected. Finally, in order to rule out alternative explanations, a tuning of the two-channel Kondo state to a one-channel Kondo state displaying Fermi liquid signatures upon breaking the degeneracy between the two frustrated screening channels, would be desirable.

The best evidence so far for generic two-channel Kondo physics has recently come from transition metal rutile nanowires [124]. In these systems, a local symmetry protects orbital two-channel Kondo behavior. In particular, the authors of Ref. [124] demonstrated that the orbital two-channel Kondo effect can be tuned to its one-channel counterpart.

An alternative strategy in realizing a two-channel Kondo effect is to employ its equivalence with other model systems. Buidling on the insight that the Kondo interaction is confined to the spin sector of the conduction electrons, Eggert and Affleck showed that magnetic impurities embedded in antiferromagnetic spin-1/2 Heisenberg chains can be mapped to the two-channel Kondo Hamiltonian [131]. More recently, Tsvelik and co-workers showed that antiferromagnetic chains coupled to clusters of spin are equivalent to a multi-channel Kondo model and would allow to access the critical scaling associated with the multi-channel Kondo effect [132].

The critical physics of the two-channel Kondo model is also equivalent to the Varma-

Jones quantum critical point [133, 134]. This quantum critical point arises in a two-impurity Kondo problem [135, 136, 137]. A general difficulty in accessing the critical point of the two-impurity Kondo model is that a direct coupling between the screening channels of the two Kondo impurities constitutes a relevant perturbation and drives the system away from criticality. The two-impurity model has been realized in an atomic point contact [138] but in such a setup, the tunneling current bypassing the two molecules must vanish before the critical point can be reached. For a review of two-impurity Kondo physics in coupled quantum dots, see Ref. [22].

Very recently, it has been argued that a periodically driven Anderson model will give rise to a two-channel Kondo effect [139]. In Ref. [140] the authors show that a three-terminal Majorana transistor, a time-reversal invariant topological superconductor attached to normal leads, can give rise to two-channel Kondo physics without the need of fine-tuning. Another very promising recent suggestion by Pustilnik and coworkers to realize the two-channel Kondo effect relies on a mesoscopic s-wave superconductor in the Coulomb blockade regime and builds on Andreev reflections [141]. Unlike the two-channel Kondo realizations in semiconductor heterostructures discussed in Section 3.2.2, there is no need for a tiny energy level spacing in this proposed setup.

Ultracold atoms in optically defined lattices have over the last decade demonstrated their potential as quantum simulator platforms of quantum many-body states [142]. Proposals to simulate the Kondo effect have been around for a few years [143]. These even include proposals to realize an orbital Kondo effect [144] and while there seems at present no confirmed realization of Kondo scattering in an ultracold cold atom setting, this may likely change in the near future [145, 146]. It therefore seems natural and indeed timely to attempt realizing the two-channel Kondo model using optically defined lattices.

References

[1] J. L. Smith, E. A. Kmetko, *J. Alloys Compd.* **1982**, *90* 83.

[2] A. C. Hewson, *The Kondo Problem to Heavy Fermions*, Cambridge University Press, Cambridge, **1993**.

[3] O. Stockert, S. Kirchner, F. Steglich, Q. Si, *J. Phys. Soc. Jpn.* **2012**, *81* 011001.

[4] F. Steglich, J. Arndt, O. Stockert, S. Friedemann, M. Brando, C. Klingner, C. Krellner, C. Geibel, S. Wirth, S. Kirchner, Q. Si, *J. Phys.: Condens. Matter* **2012**, *24*, 29 294201.

[5] I. Madan, T. Kurosawa, Y. Toda, M. Oda, T. Mertelj, D. Mihailovic, *Nat. Commun.* **2015**, *6* 6958.

[6] D. Pelc, P. Popčević, M. Požek, M. Greven, N. Barišić, *Sci. Adv.* **2019**, *5*, 1.

[7] R. Yu, P. Goswami, Q. Si, P. Nikolic, J.-X. Zhu, *Nat. Commun.* **2013**, *4* 2783.

[8] B. Keimer, S. A. Kivelson, M. R. Norman, S. Uchida, J. Zaanen, *Nature* **2015**, *518* 179186.

[9] N. E. Hussey, H. Gordon-Moys, J. Kokalj, R. H. McKenzie, *J. Phys. Conf. Ser.* **2013**, *449* 012004.

[10] P. Giraldo-Gallo, J. A. Galvis, Z. Stegen, K. A. Modic, F. F. Balakirev, J. B. Betts, X. Lian, C. Moir, S. C. Riggs, J. Wu, A. T. Bollinger, X. He, I. Božović, B. J. Ramshaw, R. D. McDonald, G. S. Boebinger, A. Shekhter, *Science* **2018**, *361*, 6401 479.

[11] J. A. N. Bruin, H. Sakai, R. S. Perry, A. P. Mackenzie, *Science* **2013**, *339*, 6121 804.

[12] J. D. Thompson, Z. Fisk, *J. Phys. Soc. Jpn.* **2012**, *81* 011002.

[13] V. Martelli, A. Cai, E. M. Nica, M. Taupin, A. Prokofiev, C.-C. Liu, H.-H. Lai, R. Yu, K. Ingersent, R. Küchler, A. M. Strydom, D. Geiger, J. Haenel, J. Larrea, Q. Si, S. Paschen, *Proc. Natl. Acad. Sci. U.S.A.* **2019**, *116*, 36 17701.

[14] M. A. Ruderman, C. Kittel, *Phys. Rev.* **1954**, *96* 99.

[15] T. Kasuya, *Prog. Theor. Phys.* **1956**, *16*, 1 45.

[16] K. Yosida, *Phys. Rev.* **1957**, *106* 893.

[17] S. Kirchner, S. Paschen, Q. Chen, S. Wirth, D. Feng, J. D. Thompson, Q. Si, *Rev. Mod. Phys.* **2020**, *92* forthcoming and arXiv:1810.13293.

[18] P. Nozières, *J. Low Temp. Phys.* **1974**, *17*, 1 31.

[19] P. Noziéres, A. Blandin, *J. Phys. (Paris)* **1980**, *41* 193.

[20] D. L. Cox, A. Zawadowski, *Adv. Phys.* **1998**, *47* 599.

[21] M. Jarrell, H. Pang, D. L. Cox, K. H. Luk, *Phys. Rev. Lett.* **1996**, *77* 1612.

[22] A. M. Chang, J. C. Chen, *Rep. Prog. Phys.* **2009**, *72*, 9 096501.

[23] P. Coleman, *Introduction to Many-Body Physics*, Cambridge University Press, **2016**.

[24] J. Kondo, *Prog. Theor. Phys.* **1964**, *32* 37.

[25] P. W. Anderson, G. Yuval, D. R. Hamann, *Phys. Rev. B* **1970**, *1* 4464.

[26] P. W. Anderson, G. Yuval, *J. Phys. C: Solid State Phys.* **1971**, *4*, 5 607.

[27] M. Fowler, A. Zawadowski, *Solid State Commun.* **1971**, *9*, 8 471 .

[28] K. G. Wilson, *Rev. Mod. Phys.* **1975**, *47* 773.

[29] P. W. Anderson, G. Yuval, *Phys. Rev. Lett.* **1969**, *23* 89.

[30] I. Affleck, A. W. Ludwig, *Nucl. Phys. B* **1991**, *360*, 2 641 .

[31] I. Affleck, A. W. Ludwig, *Phys. Rev. B* **1993**, *48* 7297.

[32] P. B. Wiegmann, *J. Phys. C: Solid State Phys.* **1981**, *14*, 10 1463.

[33] P. B. Wiegmann, A. M. Tsvelick, *J. Phys. C: Solid State Phys.* **1983**, *16*, 12 2281.

[34] N. Andrei, K. Furuya, J. H. Lowenstein, *Rev. Mod. Phys.* **1983**, *55* 331.

[35] G. Toulouse, *Phys. Rev. B* **1970**, *2* 270.

[36] R. M. Konik, H. Saleur, A. W. W. Ludwig, *Phys. Rev. B* **2002**, *66* 075105.

[37] A. Zawadowski, *Phys. Rev. Lett.* **1980**, *45* 211.

[38] H. B. Pang, D. L. Cox, *Phys. Rev. B* **1991**, *44* 9454.

[39] A. M. Tsvelick, *J. Phys. C: Solid State Phys.* **1985**, *18*, 1 159.

[40] A. M. Tsvelick, *J. Phys.: Condens. Matter* **1990**, *2*, 12 2833.

[41] J. Gan, *J. Phys.: Condens. Matter* **1994**, *6* 4547.

[42] P. Coleman, L. B. Ioffe, A. M. Tsvelik, *Phys. Rev. B* **1995**, *52* 6611.

[43] V. J. Emery, S. Kivelson, *Phys. Rev. B* **1992**, *46* 10812.

[44] A. M. Sengupta, A. Georges, *Phys. Rev. B* **1994**, *49* 10020.

[45] P. Coleman, A. J. Schofield, *Phys. Rev. Lett.* **1995**, *75* 2184.

[46] L. I. Glazman, M. E. Raikh, *JETP Lett.* **1988**, *47* 452455.

[47] T. K. Ng, P. A. Lee, *Phys. Rev. Lett.* **1988**, *61* 1768.

[48] D. Goldhaber-Gordon, J. Gres, M. A. Kastner, H. Shtrikman, D. Mahalu, U. Meirav, *Phys. Rev. Lett.* **1998**, *81*, 23 5225.

[49] S. M. Cronenwett, T. H. Oosterkamp, L. P. Kouwenhoven, *Science* **1998**, *281*, 5376 540.

[50] J. Schmid, J. Weis, K. Eberl, K. v. Klitzing, *Phys. B (Amsterdam, Neth.)* **1998**, *256-258* 182 .

[51] L. Kouwenhoven, L. Glazman, *Phys. World* **2001**, *14*, 1 33.

[52] D. Natelson, L. H. Yu, J. W. Ciszek, Z. K. Keane, J. M. Tour, *Chem. Phys.* **2006**, *324*, 1 267 .

[53] M. Pustilnik, L. Glazman, *J. Phys.: Condens. Matter* **2004**, *16*, 16 R513.

[54] G. D. Scott, D. Natelson, S. Kirchner, E. Muñoz, *Phys. Rev. B* **2013**, *87* 241104.

[55] L. Merker, S. Kirchner, E. Muñoz, T. A. Costi, *Phys. Rev. B* **2013**, *87* 165132.

[56] J. R. Schrieffer, P. A. Wolff, *Phys. Rev.* **1966**, *149* 491.

[57] F. Zamani, P. Ribeiro, S. Kirchner, *New J. Phys.* **2016**, *18* 063024.

[58] A. Taraphder, P. Coleman, *Phys. Rev. Lett.* **1991**, *66* 2814.

[59] D. C. Langreth, *Phys. Rev.* **1966**, *150* 516.

[60] J. Nygøard, D. H. Cobden, P. E. Lindelof, *Nature* **2000**, *408* 342346.

[61] L. H. Yu, D. Natelson, *Nano Lett.* **2004**, *4* 79.

[62] W. H. Appelt, A. Droghetti, L. Chioncel, M. M. Radonji, E. Muoz, S. Kirchner, D. Vollhardt, I. Rungger, *Nanoscale* **2018**, *10* 17738.

[63] A. N. Pasupathy, R. C. Bialczak, J. Martinek, J. E. Grose, L. A. K. Donev, P. L. McEuen, D. C. Ralph, *Science* **2004**, *306*, 5693 86.

[64] J. Hauptmann, J. Paaske, P. Lindelof, *Nat. Phys.* **2008**, *4* 373.

[65] S. Kirchner, L. Zhu, Q. Si, D. Natelson, *Proc. Natl. Acad. Sci. U.S.A.* **2005**, *102*, 52 18824.

[66] R. M. Potok, I. G. Rau, H. Shtrikman, Y. Oreg, D. Goldhaber-Gordon, *Nature* **2007**, *446* 167.

[67] Y. Oreg, D. Goldhaber-Gordon, *Phys. Rev. Lett.* **2003**, *90* 136602.

[68] A. J. Keller, L. Peeters, C. P. Moca, I. Weymann, D. Mahalu, V. Umansky, G. Zaránd, D. Goldhaber-Gordon, *Nature* **2015**, *526* 237.

[69] K. Matveev, *J. Exp. Theor. Phys.* **1991**, *72* 892.

[70] K. Matveev, *Phys. B (Amsterdam, Neth.)* **1994**, *203*, 3 404 .

[71] K. A. Matveev, *Phys. Rev. B* **1995**, *51* 1743.

[72] Z. Iftikhar, S. Jezouin, A. Anthore, U. Gennser, F. D. Parmentier, A. Cavanna, F. Pierre, *Nature* **2015**, *526* 233.

[73] A. Furusaki, K. A. Matveev, *Phys. Rev. B* **1995**, *52* 16676.

[74] G. Zaránd, G. T. Zimányi, F. Wilhelm, *Phys. Rev. B* **2000**, *62* 8137.

[75] Z. Iftikhar, A. Anthore, A. K. Mitchell, F. D. Parmentier, U. Gennser, A. Ouerghi, A. Cavanna, P. S. C. Mora and, F. Pierre, *Science* **2018**, *360* 1315.

[76] I. Kuzmenko, T. Kuzmenko, Y. Avishai, *Phys. Rev. B* **2014**, *90* 195129.

[77] K. Sengupta, G. Baskaran, *Phys. Rev. B* **2008**, *77* 045417.

[78] F. Zamani, T. Chowdhury, P. Ribeiro, K. Ingersent, S. Kirchner, *Phys. Status Solidi B* **2013**, *250*, 3 547.

[79] D. C. Ralph, R. A. Buhrman, *Phys. Rev. Lett.* **1992**, *69*, 14 2118.

[80] D. Ralph, R. Buhrman, *Phys. Rev. B* **1995**, *51*, 6 3554.

[81] Y. G. Naidyuk, I. K. Yanson, *Point-Contact Spectroscopy*, Springer Ser. Solid-State Sci. Springer, **2005**.

[82] E. Scheer, N. Agraït, J. C. Cuevas, A. L. Yeyati, B. Ludoph, A. Martín-Rodero, G. R. Bollinger, J. M. van Ruitenbeek, C. Urbina, *Nature* **1998**, *394*, 6689 154.

[83] S. Kirchner, J. Kroha, P. Wölfle, E. Scheer, *Anderson Localization and Its Ramifications*, volume 630 of *Lect. Notes Phys.*, chapter Conductance Quasi-quantization of Quantum Point Contacts: Why Tight Binding Models Are Insufficient, Springer, Berlin, Heidelberg, **2003**.

[84] S.-S. Yeh, J.-J. Lin, *Phys. Rev. B* **2009**, *79* 012411.

[85] P. w. Anderson, B. I. Halperin, C. M. Varma, *Philos. Mag. (1798-1977)* **1972**, *25*, 1 1.

[86] D. C. Ralph, A. W. W. Ludwig, J. von Delft, R. A. Buhrman, *Phys. Rev. Lett.* **1994**, *72* 1064.

[87] J. von Delft, D. Ralph, R. Buhrman, S. Upadhyay, R. Louie, A. Ludwig, V. Ambegaokar, *Ann. Phys. (Amsterdam, Neth.)* **1998**, *263*, 1 1 .

[88] A. Moustakas, D. Fisher, *Phys. Rev. B* **1996**, *53*, 8 4300.

[89] K. Vladár, A. Zawadowski, *Phys. Rev. B* **1983**, *28*, 3 1596.

[90] K. Vladár, A. Zawadowski, *Phys. Rev. B* **1983**, *28*, 3 1564.

[91] A. L. Moustakas, D. S. Fisher, *Phys. Rev. B* **1997**, *55* 6832.

[92] G. Zaránd, A. Zawadowski, *Phys. Rev. Lett.* **1994**, *72* 542.

[93] I. Aleiner, B. Altshuler, Y. Galperin, T. Shutenko, *Phys. Rev. Lett.* **2001**, *86*, 12 2629.

[94] I. Aleiner, D. Controzzi, *Phys. Rev. B* **2002**, *66*, 4 045107.

[95] E. Akkermans, G. Montambaux, *Mesoscopic Physics of Electrons and Photons*, Cambridge University Press, **2006**.

[96] P. A. Lee, T. V. Ramakrishnan, *Rev. Mod. Phys.* **1985**, *57* 287.

[97] J. J. Lin, J. P. Bird, *J. Phys.: Condens. Matter* **2002**, *14*, 18 R501.

[98] B. L. Altshuler, A. G. Aronov, *Electron-electron interaction in disordered conductors*, book section 1, North-Holland Physics Publishing, Amsterdam, The Netherlands, **1985**.

[99] P. Wölfle, R. N. Bhatt, *Phys. Rev. B* **1984**, *30* 3542.

[100] J. J. Lin, N. Giordano, *Phys. Rev. B* **1987**, *35* 545.

[101] L. J. Zhu, S. H. Nie, P. Xiong, P. Schlottmann, J. H. Zhao, *Nat. Commun.* **2016**, *7* 10817.

[102] L. Zhu, G. Woltersdorf, J. Zhao, *Sci. Rep.* **2016**, *6* 34549.

[103] Z. Shao, H. Zhao, J. Zeng, Y. Zhang, W. Yang, Y. Lai, S. Guo, H. Du, C. Wang, Y. Yang, J. Yang, *AIP Adv.* **2017**, *7*, 5 056213.

[104] G. Zaránd, T. Costi, A. Jerez, N. Andrei, *Phys. Rev. B* **2002**, *65* 134416.

[105] V. Aji, C. M. Varma, I. Vekhter, *Phys. Rev. B* **2008**, *77* 224426.

[106] L. J. Zhu, J. H. Zhao, *Sci. Rep.* **2017**, *7* 42931.

[107] A. Patra, K. P. Maity, R. B. Kamble, V. Prasad, *J. Phys.: Condens. Matter* **2018**, *30*, 37 375701.

[108] T. Cichorek, A. Sanchez, P. Gegenwart, F. Weickert, A. Wojakowski, Z. Henkie, G. Auffermann, S. Paschen, R. Kniep, F. Steglich, *Phys. Rev. Lett.* **2005**, *94*, 23 236603.

[109] A. Czulucki, G. Auffermann, M. Bednarski, L. Bochenek, M. Böhme, T. Cichorek, R. Niewa, N. Oeschler, M. Schmidt, F. Steglich, R. Kniep, *ChemPhysChem* **2010**, *11*, 12 2639.

[110] T. Cichorek, L. Bochenek, M. Schmidt, A. Czulucki, G. Auffermann, R. Kniep, R. Niewa, F. Steglich, S. Kirchner, *Phys. Rev. Lett.* **2016**, *117* 106601.

[111] R. N. Bhatt, P. Wölfle, T. V. Ramakrishnan, *Phys. Rev. B* **1985**, *32* 569.

[112] T. Cichorek, L. Bochenek, M. Schmidt, R. Niewa, A. Czulucki, G. Auffermann, F. Steglich, R. Kniep, S. Kirchner, *Phys. Rev. Lett.* **2017**, *118* 259702.

[113] W. Tremel, R. Hoffmann, *J. Am. Chem. Soc.* **1987**, *109*, 1 124.

[114] A. Gogolin, *Phys. Rev. B* **1996**, *53* R5990.

[115] T. Hotta, *Phys. Rev. Lett.* **2006**, *96*, 19 197201.

[116] M. Arnold, T. Langenbruch, J. Kroha, *Phys. Rev. Lett.* **2007**, *99*, 18 186601.

[117] E. F. Chuo, K. Ballmann, L. Borda, J. Kroha, *J. Phys. Conf. Ser.* **2014**, *568* 12007.

[118] G. Sellier, S. Kirchner, J. Kroha, In V. Chandrasekhar, C. V. Haesendonck, A. Zawadowski, editors, *Kondo Effect and Dephasing in Low-Dimensional Metallic Systems.* Springer Netherlands, **2001** 241–244.

[119] D. Gnida, *Phys. Rev. Lett.* **2017**, *118* 259701.

[120] D. Gnida, *Phys. Rev. B* **2018**, *97* 134201.

[121] Y. Yamane, T. Onimaru, K. Wakiya, K. T. Matsumoto, K. Umeo, T. Takabatake, *Phys. Rev. Lett.* **2018**, *121* 077206.

[122] Y. Shimura, M. Tsujimoto, B. Zeng, L. Balicas, A. Sakai, S. Nakatsuji, *Phys. Rev. B* **2015**, *91* 241102.

[123] D. L. Cox, *Phys. Rev. Lett.* **1987**, *59* 1240.

[124] S.-S. Yeh, T.-K. Su, A.-S. Lien, F. Zamani, J. Kroha, C.-C. Liao, S. Kirchner, J.-J. Lin,

Vacancy-driven multichannel Kondo physics in topological quantum material IrO_2, **2019**, ArXiv:1910.13648.

[125] S. Hoshino, Y. Kuramoto, *Phys. Rev. Lett.* **2014**, *112* 167204.

[126] R. Flint, P. Coleman, *C. R. Phys.* **2014**, *15*, 7 557 .

[127] E. Miranda, V. Dobrosavljević, G. Kotliar, *Phys. Rev. Lett.* **1997**, *78* 290.

[128] A. A. Zvyagin, *Fiz. Nizk. Temp. (Kiev)* **2002**, *28*, 12 907.

[129] E. Miranda, V. Dobrosavljević, *Rep. Prog. Phys.* **2005**, *68*, 10 2337.

[130] M. Nicklas, S. Kirchner, R. Borth, R. Gumeniuk, W. Schnelle, H. Rosner, H. Borrmann, A. Leithe-Jasper, Y. Grin, F. Steglich, *Phys. Rev. Lett.* **2012**, *109* 236405.

[131] S. Eggert, I. Affleck, *Phys. Rev. B* **1992**, *46* 10866.

[132] A. M. Tsvelik, W.-G. Yin, *Phys. Rev. B* **2013**, *88* 144401.

[133] J. Gan, *Phys. Rev. Lett.* **1995**, *74* 2583.

[134] A. K. Mitchell, E. Sela, D. E. Logan, *Phys. Rev. Lett.* **2012**, *108* 086405.

[135] B. A. Jones, C. M. Varma, *Phys. Rev. B* **1989**, *40* 324.

[136] I. Affleck, A. W. W. Ludwig, *Phys. Rev. Lett.* **1992**, *68* 1046.

[137] Y. Nishikawa, D. J. G. Crow, A. C. Hewson, *Phys. Rev. Lett.* **2012**, *108* 056402.

[138] J. Bork, Y.-H. Zhang, L. Diekhoner, L. Borda, P. Simon, J. Kroha, P. Wahl, K. Kern, *Nat. Phys.* **2011**, *7*, 11 901.

[139] M. Eckstein, P. Werner, Two-channel Kondo physics in a periodically driven single-impurity Anderson model, **2017**, ArXiv:1704.02300.

[140] Z.-Q. Bao, F. Zhang, *Phys. Rev. Lett.* **2017**, *119* 187701.

[141] M. Pustilnik, B. van Heck, R. M. Lutchyn, L. I. Glazman, *Phys. Rev. Lett.* **2017**, *119* 116802.

[142] L. Tarruell, L. Sanchez-Palencia, *C. R. Phys.* **2018**, *19*, 6 365 .

[143] J. Bauer, C. Salomon, E. Demler, *Phys. Rev. Lett.* **2013**, *111* 215304.

[144] Y. Nishida, *Phys. Rev. A* **2016**, *93* 011606.

[145] M. Kanász-Nagy, Y. Ashida, T. Shi, C. Moca, T. N. Ikeda, S. Fölling, J. I. Cirac, G. Zaránd, E. A. Demler, *Phys. Rev. B* **2018**, *97* 155156.

[146] M. Nakagawa, N. Kawakami, M. Ueda, *Phys. Rev. Lett.* **2018**, *121* 203001.